

Accepted Manuscript

Self-directed down-regulation of auditory cortex activity mediated by real-time fMRI neurofeedback augments attentional processes, resting cerebral perfusion, and auditory activation

Matthew S. Sherwood, Jason G. Parker, Emily E. Diller, Subhashini Ganapathy, Kevin B. Bennett, Carlos R. Esquivel, Jeremy T. Nelson

PII: S1053-8119(19)30285-X

DOI: <https://doi.org/10.1016/j.neuroimage.2019.03.078>

Reference: YNIMG 15754

To appear in: *NeuroImage*

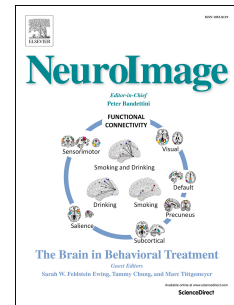
Received Date: 24 May 2018

Revised Date: 23 February 2019

Accepted Date: 31 March 2019

Please cite this article as: Sherwood, M.S., Parker, J.G., Diller, E.E., Ganapathy, S., Bennett, K.B., Esquivel, C.R., Nelson, J.T., Self-directed down-regulation of auditory cortex activity mediated by real-time fMRI neurofeedback augments attentional processes, resting cerebral perfusion, and auditory activation, *NeuroImage* (2019), doi: <https://doi.org/10.1016/j.neuroimage.2019.03.078>.

This is a PDF file of an unedited manuscript that has been accepted for publication. As a service to our customers we are providing this early version of the manuscript. The manuscript will undergo copyediting, typesetting, and review of the resulting proof before it is published in its final form. Please note that during the production process errors may be discovered which could affect the content, and all legal disclaimers that apply to the journal pertain.



1 **Self-directed down-regulation of auditory cortex activity mediated by real-**
2 **time fMRI neurofeedback augments attentional processes, resting cerebral**
3 **perfusion, and auditory activation**

4 **Matthew S. Sherwood^{1*}, Jason G. Parker², Emily E. Diller^{2,3}, Subhashini Ganapathy^{1,4}, Kevin B.**
5 **Bennett⁵, Carlos R. Esquivel⁶, Jeremy T. Nelson^{2,6,7}**

6 ¹Department of Biomedical, Industrial & Human Factors Engineering, Wright State University, Dayton, OH,
7 USA

8 ²Department of Radiology and Imaging Sciences, Indiana University School of Medicine, Indiana
9 University, IN, USA

10 ³College of Health and Human Services, Purdue University, West Lafayette, IN, USA

11 ⁴Department of Trauma Care, Boonshoft School of Medicine, Wright State University, Dayton, OH, USA

12 ⁵Department of Psychology, Wright State University, Dayton, OH, USA

13 ⁶Department of Defense Hearing Center of Excellence, JBSA-Lackland, USA

14 ⁷Ho-Chunk Inc., Alexandria, VA, USA

15 *** Correspondence:**

16 Matthew S. Sherwood,
17 Wright State University
18 413 Neuroscience Engineering Collaboration
19 3640 Colonel Glenn Highway
20 Dayton, Ohio 45435
21 E-mail: matt.sherwood@wright.edu
22 Phone: (937) 503-7178

23 **Abstract:**

24 In this work, we investigated the use of real-time functional magnetic resonance imaging (fMRI) with
25 neurofeedback training (NFT) to teach volitional down-regulation of the auditory cortex (AC) using directed
26 attention strategies as there is a growing interest in the application of fMRI-NFT to treat neurologic
27 disorders. Healthy participants were separated into two groups: the experimental group received real
28 feedback regarding activity in the AC; the control group was supplied sham feedback yoked from a random
29 participant in the experimental group and matched for fMRI-NFT experience. Each participant underwent
30 five fMRI-NFT sessions. Each session contained 2 neurofeedback runs where participants completed
31 alternating blocks of “rest” and “lower” conditions while viewing a continuously-updated bar representing
32 AC activation and listening to continuous noise. Average AC deactivation was extracted from each closed-
33 loop neuromodulation run and used to quantify the control over AC (AC control), which was found to
34 significantly increase across training in the experimental group. Additionally, behavioral testing was
35 completed outside of the MRI on sessions 1 and 5 consisting of a subjective questionnaire to assess
36 attentional control and two quantitative tests of attention. No significant changes in behavior were observed;
37 however, there was a significant correlation between changes in AC control and attentional control. Also, in
38 a neural assessment before and after fMRI-NFT, AC activity in response to continuous noise stimulation was
39 found to significantly decrease across training while changes in AC resting perfusion were found to be
40 significantly greater in the experimental group. These results may be useful in formulating effective
41 therapies outside of the MRI, specifically for chronic tinnitus which is often characterized by hyperactivity
42 of the primary auditory cortex and altered attentional processes. Furthermore, the modulation of attention
43 may be useful in developing therapies for other disorders such as chronic pain.

44 **Keywords:** fMRI, neurofeedback, neuromodulation, primary auditory cortex, attention, tinnitus

45 **Abbreviations:** EV – explanatory variable, NFT – neurofeedback training, AC – auditory cortex, A1 –
46 primary auditory cortex, CPT-X – continuous performance task, AE – attention to emotion task, pcASL –
47 pseudo-continuous arterial spin labeling

48 1. Introduction

49 The rapidly growing field of neuromodulation technology gives rise to promising technology to treat the
50 neurologic disorders by utilizing the ability to induce and/or control neural plasticity (Johnston et al., 2011;
51 Veit et al., 2012) and combating brain disorders and diseases (Hamilton et al., 2011; Vaughan et al., 2006).
52 Of the techniques currently being explored, endogenous neuromodulation techniques (Mak and Wolpaw,
53 2009; Smith et al., 2004; Sulzer et al., 2013) have the advantages of no known side effects and may be
54 translated to exercises that could be performed at home without the use of sophisticated equipment and
55 trained professionals (Caria et al., 2007; Linden et al., 2012). Real-time functional magnetic resonance
56 imaging (Cox et al., 1995; Weiskopf et al., 2007) has seen a dramatic rise in interest since its advent in 1995,
57 with a large portion of research dedicated to its application for training endogenous neuromodulation. In this
58 technique, termed closed-loop endogenous neuromodulation, the functional magnetic resonance imaging
59 (fMRI) signal is measured from a specific region of the brain, processed, and presented to the subject in real-
60 time (*i.e.*, neurofeedback). Through training, subjects develop self-directed mental processing techniques that
61 regulate this signal.

62 One such focus of fMRI neurofeedback training (fMRI-NFT) is on the treatment of tinnitus. Tinnitus, the
63 phantom perception of sound, is associated with emotional distress including anxiety and depression that can
64 have a profound effect on mental health and overall quality of life (Halford and Anderson, 1991; Jun and
65 Park, 2013), and was the main motivation of this work. The neural mechanisms of tinnitus are not well
66 understood but have been studied using various techniques. Although there is no cure for tinnitus, there is a
67 rapidly-expanding portfolio of treatment options that include pharmacologic, behavioral, and
68 neuromodulatory strategies. Tinnitus treatments are categorized almost universally as treating 1) the tinnitus
69 percept (*i.e.*, the neural mechanisms responsible for the rise of the percept) or 2) the tinnitus affect (*i.e.*, the
70 emotional response). Pharmacologic and behavioral therapies make up the majority of treatment strategies
71 for tinnitus patients, but both currently target the tinnitus affect.

72 Neuromodulatory techniques attempt to correct abnormal neural patterns of the brain. In the case of tinnitus,
73 the target is often the auditory cortex (AC), which has been shown to be hyperactive in fMRI studies (Gu et
74 al., 2010; Seydell-Greenwald et al., 2012) and have elevated steady-state metabolism in positron emission
75 tomography studies (Langguth et al., 2006; Schecklmann et al., 2013; Wang et al., 2001). Using fMRI-NFT,
76 internal stimulation is utilized to potentially target either the tinnitus percept or affect (Folmer et al., 2014).
77 Three previous studies have investigated the effect of control over the activation of the AC learned from
78 fMRI-NFT on is achievable without concurrent auditory stimulation during attempted control. In the first
79 controlled study, it was indicated that healthy individuals can learn to control the activated cortical volume in
80 the primary and secondary auditory cortex using fMRI-NFT (Yoo et al., 2006). In the second study, it was
81 reported that control over the magnitude of A1 activation is achievable in a cohort of tinnitus patients (Haller
82 et al., 2010). However, this study was not controlled so this finding could not be necessarily attributable to
83 fMRI-NFT and subjective measures of tinnitus were not statistically analyzed. More recently, Emmert et al.
84 (2017) demonstrated the capacity of tinnitus patients to down-regulate the auditory cortex using continuous
85 and intermittent neurofeedback. Single-session results identified greater down-regulation in the intermittent
86 feedback group; but over multiple sessions, the continuous feedback was more advantageous. There were no
87 reported changes in resting cerebral blood perfusion within the auditory cortex; however, there was a
88 significant decrease in the relaxation sub-score of the tinnitus functional index indicating relaxation capacity
89 was less impacted by tinnitus.

90 In the work presented here, we translated our previous work investigating control over the prefrontal cortex
91 using fMRI-NFT and cognitive abilities (Sherwood et al., 2016a; 2016b) to teach volitional down-regulation
92 of the AC during binaural auditory stimulation using directed attention strategies. Our goal of this work is to

93 demonstrate the possibility of subjects to endogenously down-regulate AC activity in the presence of a
94 controlled stimulus and relate this to behavior; therefore, healthy subjects were selected for this study.

95 **2. Methods**

96 2.1 Participants

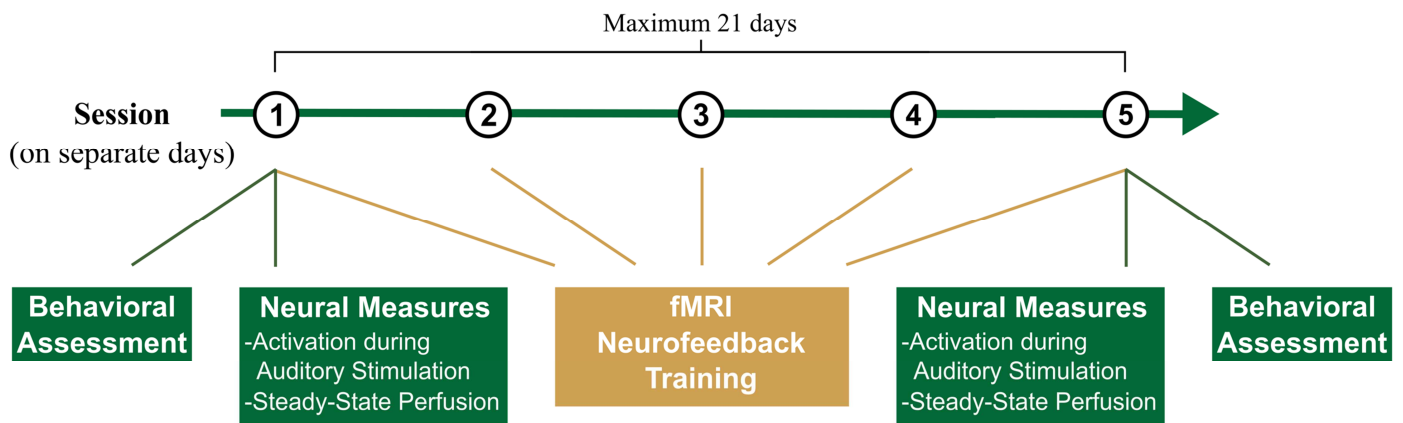
97 This study utilized healthy volunteers recruited from Wright State University and the surrounding
98 community. Each participant completed a telephone screening to qualify for the study. Forty-one participants
99 randomly selected from the qualifying pool were enrolled for further screening. Written informed consent
100 was obtained from each participant prior to any experimental procedures which were approved by Wright
101 State University's Institutional Review Board (IRB) and the Air Force Medical Support Agency Surgeon
102 General's Research Oversight Committee. Participants that were eligible for compensation received equal
103 remuneration.

104 The participants were randomly assigned to one of two groups. Both groups received the same instructions
105 and performed the same tasks with the exception of the authenticity of the feedback during endogenous
106 closed-loop neuromodulation. In the experimental group (EXP), real feedback was provided while sham
107 feedback was utilized in the control group (CON). Participants in each group were blinded to the validity of
108 the feedback. In total, thirteen (4 CON, 9 EXP) participants voluntarily withdrew for unknown reasons or
109 were withdrawn from the study due to excessive motion, absenteeism/tardiness, or software/hardware issues
110 that limited the completion of study procedures. Of these thirteen, 6 (3 CON) gave written, informed consent
111 but did not complete any experimental sessions, four (1 CON) were removed after a single session due to
112 excessive motion (3) or unknown reasons (1), two participants were withdrawn after 2 sessions, and the last
113 participant was withdrawn after 4 sessions due to the inability to complete the fifth session within the 21-day
114 timeframe. Furthermore, the MRI data for a single EXP participant was corrupted and excluded from the
115 analysis. The presented results represent the remaining twenty-seven participants: eighteen EXP participants
116 (mean age 23.2 +/- 1.1, 11 males) and nine CON participants (mean age 24.4 +/- 2.5, 4 males). This
117 imbalance was maintained by design to complete the objectives of the funded work while maintaining a
118 controlled design to properly evaluate the effects of the study.

119 2.2 Experimental design

120 An overview of the experimental design is shown in Figure 1. All participants first completed a preliminary
121 visit where informed consent was obtained. After consenting to the experiment, the participants completed a
122 few demographic forms and a standard MRI screening form. Prior to familiarizing the participants with the
123 testing apparatus, a short hearing test was conducted using a mobile audiometry system (Shoebox
124 Audiometry, Ontario, Canada) with calibrated transducers (HDA 280, Sennheiser, Wedemark, Deutschland).
125 This was conducted in a standard laboratory setting to verify normal hearing, determined by no frequencies
126 with a hearing threshold above 40 dB on a standard audiogram to ensure a normal, healthy auditory system.
127 The implemented hearing test was a simple, self-applied examination that has been clinically validated
128 (Saliba et al., 2016; Thompson et al., 2015).

129 The remaining experimental procedures were completed across five sessions completed within 21 days and
130 no more than one per day. The first session began with a behavioral assessment followed by an assessment of
131 neural measures and fMRI-NFT. The second, third, and fourth sessions only consisted of fMRI-NFT. The
132 fifth session began with fMRI-NFT, followed by an assessment of neural measures and a behavioral
133 assessment. All neural assessments and fMRI-NFT procedures were performed inside the MRI scanner while
134 the behavioral assessments were completed outside of the MRI.



135

136

137

138

139

Figure 1. Overview of the experimental design. The first session began with an initial assessment of behavior and neural measures followed by fMRI-NFT. The second, third, and fourth sessions consisted of only fMRI-NFT. The fifth session started with fMRI-NFT followed by a second assessment of neural measures and behavior.

140

2.3 Image Data Acquisition

141

142

143

144

145

146

147

148

149

150

All MRI procedures were conducted on a 3 Tesla (T) MRI (Discovery 750W, GE Healthcare, Madison, WI) using a 24-channel head coil. fMRI data (T2*-weighted) were collected using a gradient-recalled-echo (GRE) sequence sensitive to the BOLD signal. This sequence acquired data using the following parameters: 64 x 64 element matrix, 41 slices oriented parallel to the AC-PC plane, 3.5 x 3.5 x 3 mm³ voxel size, 0.5 mm slice gap, 2000 ms repetition time (TR), 20 ms echo time (TE), a flip angle of 90°, and fat suppression was enabled. In previous unpublished data, these parameters were shown to reduce susceptibility artifacts which can be significant at high field strengths such as 3T. TE was chosen to allow for high SNR in the cortex while minimizing the effects of susceptibility in deeper structures associated with attentional control, including the ventromedial prefrontal cortex (Fera et al., 2004; Hyde et al., 2001; Shinozaki et al., 2013; Wager et al., 2011).

151

152

153

154

155

156

Structural (T1-weighted) images were acquired using a 3D brain volume imaging (BRAVO) pulse sequence imploring an inversion recovery prepared fast spoiled gradient-echo (FSPGR). The structural images were acquired using a 256 x 256 element matrix, 172 slices oriented in the same plane as the functional scans, 1 mm³ isotropic voxels, 0.8 phase field of view factor, inversion time (TI) = 450 ms, TE = 3.224 ms, a flip angle of 13°, and an auto-calibrated reconstruction for Cartesian sampling with a phase acceleration factor of 2.0.

157

158

159

160

161

162

163

164

165

166

167

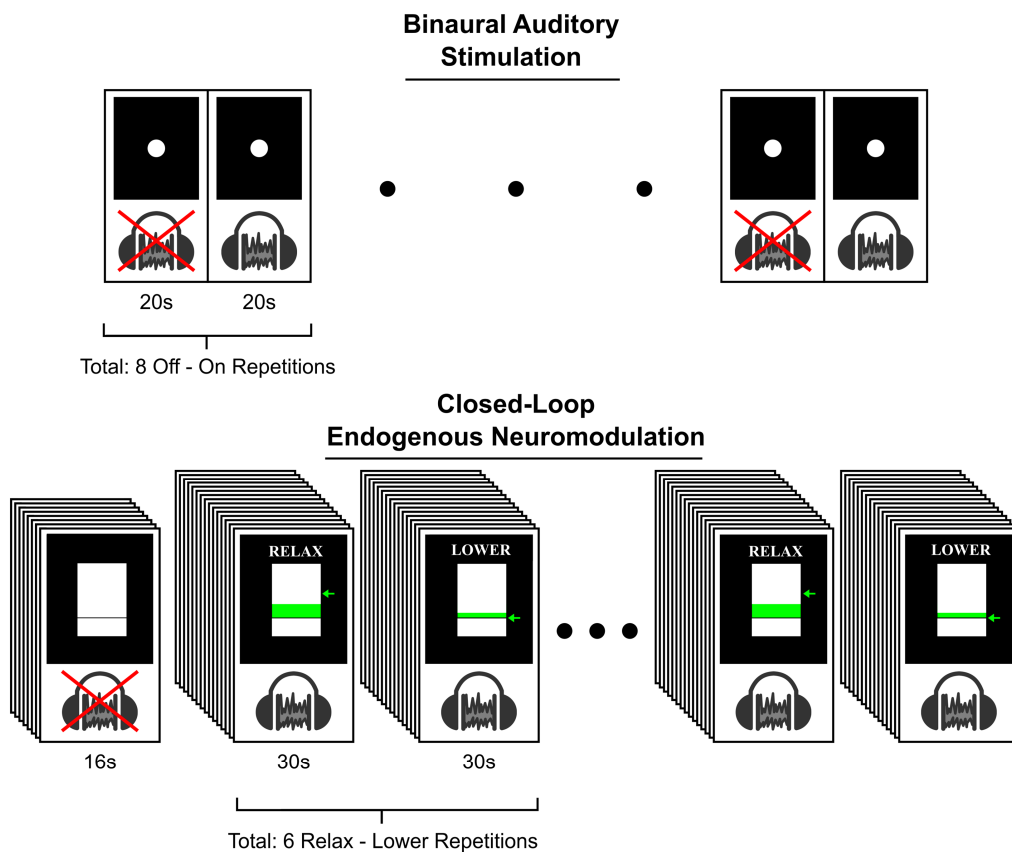
Images of cerebral perfusion were acquired using a pseudo-continuous arterial spin labeling (pcASL) technique (Silva and Kim, 1999) with inversion (tagging) pulses administered immediately inferior to the imaging volume. All acquisitions used a post-label delay time (PLD) of 2025 ms. Five background suppression pulses were applied to reduce the signal of stationary tissues (Dixon et al., 1991; Mani et al., 1997; Ye et al., 2000) and improve signal-to-noise ratio (SNR) of arterial blood. A 3D fast spin echo (3D FSE) sequence was used for acquisition of the imaging volume. To reduce motion sensitivity, improve acquisition time, and minimize susceptibility artifacts, a stack-of-spirals readout gradient starting at the center of k-space was used (Glover, 2012). A total of 8 spiral arms were used for k-space sampling. Echoes were re-binned to Cartesian space in a 128x128 matrix, with TR = 4640 ms, TE = 10.7 ms, voxel size = 1.875 x 1.875 mm, slice thickness = 4 mm, and flip angle = 111°. The sequence acquired a total of 3 tag/control pairs with a total acquisition time of 4 min 46 s. During the scan, participants were instructed to

168 remain awake and focus on a fixation dot presented on the display. This condition has demonstrated
169 significantly greater reliability in resting-state functional MRI across all within-network connections, as well
170 as within default-mode, attention, and auditory networks when compared to eyes open (no specified fixation)
171 and closed methods (Patriat et al., 2013).

172 2.4 fMRI-NFT

173 Prior to entering the MRI environment, MRI screening forms were reviewed by a registered MRI technician.
174 Female participants were required to take a urine dipstick pregnancy test. Once entering the MRI, the
175 participants first inserted MRI-compatible ear plugs (MagnaCoil, Magnacoustics Inc., Atlantic Beach, NY)
176 capable of providing communication and auditory stimulation (Genesis Ultra, Magnacoustics Inc., Atlantic
177 Beach, NY). Next, the participants were positioned supine on the MRI table, their head was padded to
178 restrict motion, and the upper part of the 24-channel head coil was attached. Using a laser, the nasion was
179 landmarked relative to the MRI. The landmarked position was moved to the center of the MRI bore.

180 Once positioned, the fMRI-NFT procedures began (Figure 2). Each fMRI-NFT session consisted of a single
181 run of bilateral auditory stimulation which was used to individually and functionally localize the AC. This
182 scan is referred to as the “functional localizer”, followed by two runs of attempted self-regulation
183 supplemented with neurofeedback from the AC (referred to as closed-loop endogenous neuromodulation).
184 Between the functional localizer and the closed-loop endogenous neuromodulation runs, a structural MRI
185 was acquired. During this time, the left and right AC were manually identified using anatomical markers and
186 an activation map produced from the functional localizer. Once identified, a volume-of-interest (VOI) was
187 selected to determine the voxels utilized to generate the subsequent neurofeedback.



188

189 Figure 2. Overview of each fMRI-NFT session. Each session began by acquiring BOLD data during a
 190 blocked binaural auditory stimulation paradigm. Next, a volume-of-interest for subsequent neurofeedback
 191 was selected from activated voxels in the right and left AC. Finally, two runs of closed-loop endogenous
 192 neuromodulation were executed to train AC down-regulation.

193 2.4.1 Binaural auditory stimulation

194 To identify the AC, a single run of binaural auditory stimulation was executed in a boxcar design with six (6)
 195 repetitions of OFF and ON blocks. The auditory stimulus was 10 kHz lowpass filtered white noise (Gu et al.,
 196 2010) with a 6 dB rolloff and a 0.5 s fade-in (Audacity 2.1.3, www.audacity.org). Broadband noise was
 197 chosen to minimize variation in AC signal response across subjects who were controlled for overall hearing
 198 loss, but not for tonal-specific deficiencies. Although robust across patients, this approach may not be
 199 optimal for delineation of the AC as it has been shown that EPI sequence noise is similar to a complex tone
 200 embedded in broadband noise (Langers and van Dijk, 2011; Langers et al., 2014a). The duration of each
 201 block was 20 s, and the first block began after the acquisition of four (4) dummy volumes and one (1)
 202 software preparation volume. Binaural auditory stimulation was delivered via the headphones only during
 203 ON blocks and controlled via a stimulus presentation software (Presentation, Neurobehavioral Systems, Inc.,
 204 Berkeley, CA). A continuous scan protocol was chosen to minimize differences between the AC localization
 205 procedure and subsequent NFT, although it has been shown that sparse scan designs can produce overall
 206 better localization of the AC (Langers et al., 2014b). The participants were not required to respond in any
 207 way during the scan, however they were instructed to remain awake and to focus on a round fixation dot
 208 presented in gray with a black background on a MRI-compatible display (SensaVue, Invivo, Gainesville,
 209 FL).

210 2.4.2 VOI selection

211 Immediately following acquisition, the BOLD data were pre-processed using custom MATLAB and C++
212 software. The pre-processing included standard spatial filtering (3D, 5-point Gaussian low-pass kernel, full-
213 width half-maximum of 7 mm), motion correction (corrected to the first volume using a rigid-body 3-
214 parameter model) and temporal filtering (5-point Gaussian low-pass kernel, sigma of 3 s) processing
215 functions (Friston et al., 1995).

216 An activation map was created by defining a single explanatory variable (EV) by convolving a boxcar model
217 containing 20 s control and task conditions with a pre-defined HRF (Ashby, 2011). Next, the BOLD data at
218 each voxel was fit to the model using a general linear model (GLM) by applying a weight of +1 to the EV,
219 representative of activation (positive correlation to the model). The resulting β parameter maps were
220 converted to t statistic maps (activation maps) using standard statistical transforms. The region in the AC in
221 which the feedback signal for the subsequent closed-loop endogenous neuromodulation runs was derived
222 from this activation map. Voxels were added to the auditory VOI by first locating the axial slice in which the
223 inferior surface of the anterior ventricle horns are visible. Then, activation patterns on the left and right
224 hemispheres near the posterior end of the lateral sulci were observed in this slice and the slices immediately
225 inferior and superior to the slice containing the inferior surface of the anterior ventricle horns. The t statistic
226 threshold was adjusted to reveal approximately 10-15 connected voxels per hemisphere across these three
227 slices. Voxels surviving this threshold and located within these regions were added to the VOI to complete
228 the determination of the functional localizer.

229 2.4.3 Closed-loop endogenous neuromodulation

230 Following the functional localizer, two runs of closed-loop endogenous neuromodulation were completed.
231 Four dummy volumes and one software preparation volume were acquired first. Then, eight volumes were
232 acquired to determine a baseline BOLD signal value for the selected auditory VOI. During the acquisition of
233 the baseline volumes, a countdown was displayed on the screen beginning at 16 s; however, there was no
234 auditory stimulation during either the eight baseline volumes or the four preparatory volumes.

235 After baseline, six repetitions of 30 s relax and lower blocks were completed in a boxcar-design. Both blocks
236 were accompanied with binaural auditory stimulation using the same continuous noise from the functional
237 localizer. During relax, every participant was instructed to relax and clear their mind, resulting in an increase
238 in the feedback signal. They were also instructed to keep their eyes open. Participants were instructed to
239 lower the feedback signal during lower blocks by performing a mindfulness task wherein they should
240 decrease brain activity associated with auditory input. A list of four example mindfulness tasks were
241 provided, giving the participants a few starting points.

242 During these relax and lower plots, a feedback signal was computed and displayed to the EXP participants
243 from real-time analyses of BOLD data. These real-time analyses were implemented in custom MATLAB and
244 C++ software and included standard spatial filtering (3D, 5-point Gaussian low-pass kernel, full-width half-
245 maximum of 7 mm) and motion-correction (corrected to the first volume of the functional localizer using a
246 rigid-body 3-parameter model) processing functions (Friston et al., 1995). This custom software further
247 compared the average BOLD signal in the auditory VOI during the 8 baseline volumes to that of the current
248 volume to derive a percent signal change. The current feedback signal was determined by temporally-
249 filtering (5-point Gaussian low-pass kernel consisting of only past components, sigma of 3 s) the percent
250 BOLD signal change with the feedback signals from previous volumes.

251 This feedback signal was presented to the participants using a thermometer-style bar plot where the height of
252 the bar was proportional to the percent signal change from baseline. A change of 1% in the BOLD signal
253 resulted in a bar height of 1° visual angle. Furthermore, an arrow appeared to the right of the bar plot to act

254 as a target line for the feedback bar. During relax blocks, the arrow was placed at a height equivalent to 1%
255 as the auditory VOI BOLD signal should increase relative to baseline due to the auditory stimulation. In the
256 lower blocks, the arrow appeared at a height equivalent to 0% tasking the participants with lowering the
257 auditory VOI response to the auditory stimulation to the level when no stimulation is provided. Task
258 instructions (*i.e.*, relax and lower) indicating the current block were additionally supplied above the
259 thermometer plot. For participants in the control group, the feedback display and instructions were
260 equivalent to the EXP group but the feedback signal used to determine the height of the feedback bar was
261 yoked from a random EXP participant but matched for experimental progress. Both runs from each session
262 were duplicated from the same EXP participant but the EXP participant was selected randomly each session.
263 The goal of the feedback was for participants to learn mindfulness tasks that are most successful in
264 regulating the auditory cortex.

265 2.5 Behavioral Assessment

266 Behavioral measures of attentional control were collected using one questionnaire and two computerized
267 tasks. These tasks were conducted using a laptop outside of the MRI. The participants wore active noise-
268 cancelling headphones (Samsung Level, Samsung Electronics America, Ridgefield Park, NJ) to mitigate
269 distracting sounds during the tasks. The questionnaire provided subjective measures of attentional control
270 while the computerized tasks provided objective measures. The attentional control scale (ACS; Derryberry
271 and Reed, 2002) was completed using digitized version (Qualtrics, Provo, UT) to measure the general
272 capacity for attentional control. Sub-factors of the ACS include measures of the ability to focus attention,
273 shift attention between tasks, and flexibly control thought.

274 The attention to emotion task (AE; Harris and Pashler, 2004; Moray, 1959) requires participants to make a
275 speedy judgement about the parity of two digits separated by a word. In a limited number of scattered trials,
276 response times are significantly slowed when the word is the participant's own name evaluating the impact
277 of emotion of attention. Harris and Pashler (2004) found that when a person's name or an emotionally
278 charged stimulus is presented, the stimulus may or may not be enough to warrant recognition likely subject
279 to the attentional capacity limitations found in similar tasks utilizing more "ordinary" stimuli. We
280 implemented this task to determine the influence of, if any, fMRI-NFT on attentional control. The AE task
281 was controlled via a stimulus presentation software (Presentation, Neurobehavioral Systems, Inc., Berkeley,
282 CA). One hundred and thirty trials were executed, each beginning with a gray fixation point presented for
283 500 ms. The stimuli followed the fixation and consisted of two digits (1-9) in gray flanking a word presented
284 in green. The stimuli were presented for 150 ms. Neutral (*i.e.*, ordinary) words appeared in 100 trials and 30
285 trials contained the participant's name (*i.e.*, emotionally-charged stimulus). No neutral words were repeated
286 within a single session. After the stimulus, there was a feedback period with a duration dependent upon the
287 response time. The feedback period was limited to a minimum of 500 ms and maximum of 5000 ms.
288 Participants were to use this time to indicate whether the digits were both even or odd (left control button) or
289 mismatched (right control button). Half of the name and half of the neutral trials mismatched, the other half
290 matched. The trials were randomized apart from the first fifteen trials which contained only neutral trials.
291 Finally, a 1000 ms inter-trial interval (ITI) separated the start of the next trial and the preceding response.

292 The continuous performance test (CPT) was developed to measure deficits in sustained attention (Chen et al.,
293 1998). A variant of the CPT was developed as a simultaneous discrimination and vigilance task (CPT-X).
294 The CPT-X uses a single character or number as a target and a response is inhibited when the stimulus
295 matches the target. This task was implemented to measure sustained attention and vigilance. The CPT-X
296 contained 300 trials separated evenly across four continuous blocks controlled via the stimulus presentation
297 software. Each block contained 15 matching trials and 60 non-matching trials. The order of the stimuli was

298 randomized within each block. The stimuli consisted of capitalized letters from the English alphabet with ‘X’
299 being the target. Participants were instructed to press the right control button when the stimulus did not
300 match the target and inhibit this response when the stimulus matched the target. The stimulus was presented
301 for 500 ms in gray upon a black background. An ITI randomly sampled from 500, 700, and 900 ms separated
302 each stimulus to prevent participants from predicting the presentation of stimuli. During this period, a gray
303 fixation point was presented on a black background.

304 2.6 Neural Assessment

305 The single run of binaural auditory stimulation was utilized to assess changes in the neural auditory response.
306 This was executed during prior to closed-loop endogenous neuromodulation as part of fMRI-NFT but was
307 also repeated after fMRI-NFT on the fifth session. Additionally, a baseline measure of steady-state perfusion
308 was acquired during the first session prior to fMRI-NFT. A second measure of steady-state perfusion was
309 collected during the last session following fMRI-NFT. During this scan, participants were instructed to
310 remain awake and to focus on the focal point displayed on the screen.

311 2.7 Data Analysis

312 2.7.1 Closed-loop endogenous neuromodulation

313 The BOLD data acquired from each closed-loop endogenous neuromodulation run was processed using the
314 FMRIB Software Library (FSL; Smith et al., 2004; Woolrich et al., 2009). First, individual (first-level)
315 analyses were conducted on each of the 4D fMRI data sets. Prior to the individual analyses, pre-processing
316 was performed using standard techniques. These consisted of applying a high-pass temporal filter (Gaussian-
317 weighted least-squares straight line fitting, cut-off = 60 s) to each voxel, correcting for motion by registering
318 each volume to the center volume of the data set (rigid-body 12-parameter model; Jenkinson et al., 2002),
319 creating a brain mask from the first volume and applying to each subsequent volume (Smith, 2002), spatial
320 filtering on each volume using Gaussian convolution (full-width half-maximum of 5.625 mm), and removing
321 low-frequency trends using a local fit of a straight line across time at each voxel with Gaussian weighting
322 within the line to create a smooth response.

323 Next, individual analyses were conducted on each of the 4D fMRI data sets. A single EV was defined by
324 convolving a boxcar model containing 30 s rest and task conditions with a hemodynamic response function
325 (HRF; modeled by a gamma function; phase offset = 0 s, standard deviation = 3 s, mean lag = 6 s). The
326 temporal derivative of the original waveform was added to the result and the temporal filter used in pre-
327 processing was applied. The data set was fit to the model using a general linear model (GLM) with
328 prewhitening by applying a weight of -1 to the EV, representative of de-activation during closed-loop
329 endogenous neuromodulation (negative correlation with the model). Z statistic maps were created using
330 standard statistical transforms to convert the β parameter maps. A clustering method allowed us to account
331 for false positives due to multiple comparisons. This method considers adjacent voxels with a z statistic of
332 2.3 or greater to be a cluster. The significance for each cluster was estimated and compared to a threshold of
333 $p < 0.05$ using Gaussian Random Field theory. The significance of voxels that either did not pass the
334 significance level threshold or do not belong to a cluster were set to zero. A mean image of the data set was
335 registered to the individual’s high-resolution structural image by estimating motion from a boundary-based
336 registration method including a fieldmap-based distortion correction (Greve and Fischl, 2009), then further
337 registered to the MNI-152 T1-weighted 2 mm template provided in FSL (Collins et al., 1995; Mazziotta et
338 al., 2001) using a 12-parameter model (Jenkinson et al., 2002; Jenkinson and Smith, 2001). The z statistic
339 maps were converted to standard space using the transform responsible for morphing the mean image of each
340 data set to the template to co-register all volumes.

341 Next, we performed a VOI analysis to determine each participants ability to down-regulate the auditory
 342 cortex. We converted the target VOI coordinates from each fMRI-NFT session to a binary mask. Since the
 343 VOI was determined from the first volume of the functional localizer, motion was corrected in the functional
 344 localizer data by registering each volume to the first volume using the method described above and creating a
 345 mean image. Next, the mean image of each neuromodulation run was registered to the mean image of the
 346 associated functional localizer using a rigid-body 12-parameter model. The transform responsible for
 347 morphing the mean image of each neuromodulation run was applied to the associated VOI mask. AC down-
 348 regulation was assessed in both groups by masking the cluster-corrected de-activation map from above with
 349 the registered VOI mask. A 2x2 (between-subjects factor: group; within-subjects factors: session and run)
 350 repeated measures ANOVA was performed on AC down-regulation using SPSS (IBM SPSS statistics
 351 version 24.0, IBM Corp., Amonk, New York) to compare the overall change in volitional control from
 352 session 1 run 1 to session 5 run 5.

353 Finally, we performed a voxel-based group (second level) analysis using the results of the first level. A 2x2
 354 (between subject factor: group; within-subjects factor: session) repeated measures ANOVA was
 355 implemented in FSL with a mixed-effects method. Runs 1 and 2 from the first and last fMRI-NFT session
 356 were included to assess the overall changes associated with learning down-regulation of the AC. Prior to
 357 running this analysis, each individual de-activation map was masked to remove activated voxels. This
 358 enabled us only to assess changes in de-activation as the results of the ANOVA are bi-directional. The
 359 ANOVA analysis assumed the covariance between measures within-subject follow a compound symmetric
 360 structure (equal variance and intra-subject correlations being equal). This assumption is valid as the data was
 361 acquired in close proximity and regularly sampled. Two contrasts were created to identify voxels with
 362 stronger de-activation during the fifth training session than the first session and a larger change in de-
 363 activation from the first to fifth training session ($5 - 1$) for the EXP group when compared to the CON group.
 364 Z statistic maps, created by transforming the resulting β parameter maps using standard statistical transforms,
 365 were thresholded using the clustering method outlined above with a z statistic threshold of 1.96.
 366 Furthermore, β parameter estimates from each of these contrasts underwent separate F tests to explore the
 367 main effect of session and the session by group interaction. This analysis lacked the degrees of freedom
 368 necessary to include the main effect of group and, therefore, this contrast was not included. Z statistic images
 369 were created from F statistic images using standard statistical transformations.

370 2.7.2 Behavioral assessment

371 The ACS total score was computed for each participant/session by summing the scores from the responses. A
 372 2x2 repeated measures ANOVA (between-subjects factor: group; within-subjects factor: session) was
 373 completed in SPSS on the ACS total score to assess changes across pre- and post-training assessments. *Post*
 374 *hoc*, Bonferroni-corrected pairwise comparisons were conducted on significant interaction effects.

375 The AE was analyzed to measure latency (*i.e.*, response time) to determine the effect of emotionally-charged
 376 stimuli on response time as a measure of distractibility and attentional control whereas if emotionally-
 377 charged stimuli should increase the response time (*i.e.*, distract) then attentional control is lower. Each trial
 378 was categorized as correct or incorrect. Mean latency was determined for the correct responses from each
 379 type (emotional or neutral) and session. A test statistic to analyze for outliers was performed using the
 380 following equation:

$$381 \quad T1 = \frac{x(n)-x}{s} \quad (1)$$

382 where $x(n)$ is the latency of a single observation, x is the mean latency, and s is the standard deviation. The
 383 test statistic was compared to a critical value of 3.27 (Lovie, 1986). A final mean latency was recalculated by
 384 using the latencies with test statistics less than the critical value. To determine a measure inversely related to

385 attentional control, the difference between the mean emotional and neutral latencies were computed as a
 386 percent change (Δ AE mean latency).

387 Assessment of the CPT-X was founded upon signal detection theory (SDT; Green and Swets, 1966). Each
 388 trial was separated into one of four possibilities according to SDT: 1) target was not present and the response
 389 was indicated (*i.e.*, correct rejection), 2) target was present and the response was inhibited (*i.e.*, hit), 3) target
 390 was not present and the response was inhibited (*i.e.*, false alarm), and 4) target was present and the response
 391 was indicated (*i.e.*, miss). Using the hit and false alarm rates from each session, an index of sensitivity (d' ,
 392 *i.e.*, discriminability) was computed using the procedures previously verified (Sorkin, 1999). Sensitivity is
 393 desirable as it is free from motivational effects (Swets and Sewall, 1963). In summation, this process finds
 394 the z scores for which the standard normal cumulative distribution equals the hit and false alarm rates. The z
 395 score for the false alarm rate became indeterminate when the no false alarms were made, which was the case
 396 in several sessions. Therefore, a corrected false alarm rate was calculated when no false alarms were present
 397 using the equation:

$$398 \quad 1 - 2^{-1/t} \quad (2)$$

399 where t is the number of correct rejection trials. Then, d' is calculated as the difference between the z score
 400 for the hit and false alarm rate ($z_{\text{hit}} - z_{\text{false_alarm}}$).

401 2x2 repeated measures ANOVAs similar to that described for ACS total score were also completed on Δ AE
 402 mean latency and CPT-X sensitivity separately to assess changes across pre- and post-training assessments.
 403 *Post hoc*, Bonferroni-corrected pairwise comparisons were conducted on significant interaction effects. The
 404 ANOVAs were all completed using SPSS. In the ANOVAs, Mauchly's Test of Sphericity could not be
 405 conducted on the within-subjects factors because there were only single differences to compute between
 406 factor levels and, therefore, no comparison to be made so sphericity was assumed.

407 2.7.3 Binaural auditory stimulation

408 The BOLD data from the session 1 pre-NFT and session 5 post-NFT binaural auditory stimulation runs
 409 underwent similar processing as the closed-loop endogenous neuromodulation runs. The pre-processing was
 410 the same with the exception of the high-pass temporal filter which used a cut-off of 40 s. After pre-
 411 processing, a single EV was defined by convolving a boxcar model containing 20 s rest and task conditions
 412 with the HRF. The temporal derivative of the original waveform was added to the result and the temporal
 413 filter described above was applied to the model. The data were fit to the model using a GLM with
 414 prewhitening by applying a weight of +1 to the EV, representative of activation during the task (positive
 415 correlation with the model). Z statistic maps were created using standard statistical transforms to convert the
 416 β parameter maps. The clustering method outline above was implemented with a z statistic threshold of 2.3.
 417 A mean image of the data was registered to the individual's high-resolution structural image by estimating
 418 motion from a boundary-based registration method including a fieldmap-based distortion correction, then
 419 further registered to the MNI-152 T1-weighted 2 mm template provided in FSL using a 12-parameter model.
 420 The z statistic maps were then converted to standard space using the transform responsible for morphing the
 421 mean image of each data set to the template to co-register all volumes.

422 Group (second level) analyses were performed in FSL using to conduct 2x2 (between subject factor: group;
 423 within-subjects factor: session) repeated measures ANOVAs on a voxel-by-voxel basis in FSL with a mixed-
 424 effects method. Again, the data was acquired close in proximity and regularly samples, validating the
 425 assumption of compound symmetry. Two contrasts were created to identify voxels more active during the
 426 session 5 post-NFT than session 1 pre-NFT and a larger change in activation between these runs for the EXP
 427 group than the CON group. Z statistic maps, created by transforming the resulting β parameter maps using
 428 standard statistical transforms, were thresholded using the clustering method outlined above with a z statistic

429 threshold of 1.96. Furthermore, β parameter estimates from each of these contrasts underwent separate F
430 tests to explore the main effect of session and the session by group interaction. This analysis lacked the
431 degrees of freedom necessary to include the main effect of group, therefore this effect was not included. Z
432 statistic images were created from F statistic images using standard statistical transformations.

433 2.7.4 Steady-State Perfusion

434 Steady-state perfusion was assessed from ASL to quantify CBF, measured in units of mL/100 mg/min.
435 Calculation of CBF maps was performed using automated functions in the GE reconstruction software. First,
436 the 3 tagged and 3 control volumes were first averaged in place (without motion correction). Then,
437 difference images were calculated for all patients by subtracting the average tagged volume from the average
438 control volume automatically. Finally, quantitative CBF maps were generated from the difference images,
439 the proton density (PD) weighted volumes, and a standard single compartment model (Alsop et al., 2015;
440 Alsop and Detre, 1996; Mutsaerts et al., 2014). Data from two (2) participants (1 CON, 1 EXP) were
441 corrupted, thus the analysis includes the remaining 8 CON and 17 EXP participants.

442 The CBF maps from each day and session run were processed using the FSL on a 74-core Rocks Cluster
443 Distribution (www.rocksclusters.org) high-performance computing system capable of running 120 threads in
444 parallel. First, individual (first-level) analyses were conducted on each of the CBF maps. The PD-weighted
445 images acquired were registered to the individual's high-resolution structural image by estimating motion
446 from a boundary-based registration method including a fieldmap-based distortion correction, then further
447 registered to the MNI-152 T1-weighted 2 mm template provided in FSL using a 12-parameter model. The
448 CBF maps were converted to standard space using the transform responsible for morphing the PD-weighted
449 image of each data set to the template in order to co-register all volumes.

450 Next, group non-parametric statistical analyses were performed on the session 1 pre-NFT and session 5 post-
451 NFT co-registered CBF maps using permutation testing implemented using FSL randomise (Anderson and
452 Robinson, 2001; Winkler et al., 2014). Due to our mixed-model design, we were not able to perform an
453 analysis of variance (ANOVA) using this approach. Instead, two separate analyses were performed. In the
454 first approach, an analysis was conducted across training combining the two groups to evaluate the effect of
455 session. Null t distributions for contrasts representative of the main effect of session were derived by
456 performing 1,000,000 random permutations (Nichols and Holmes, 2003). A clustering method described in
457 the group analysis above allowed us to account to false positives due to multiple comparisons.

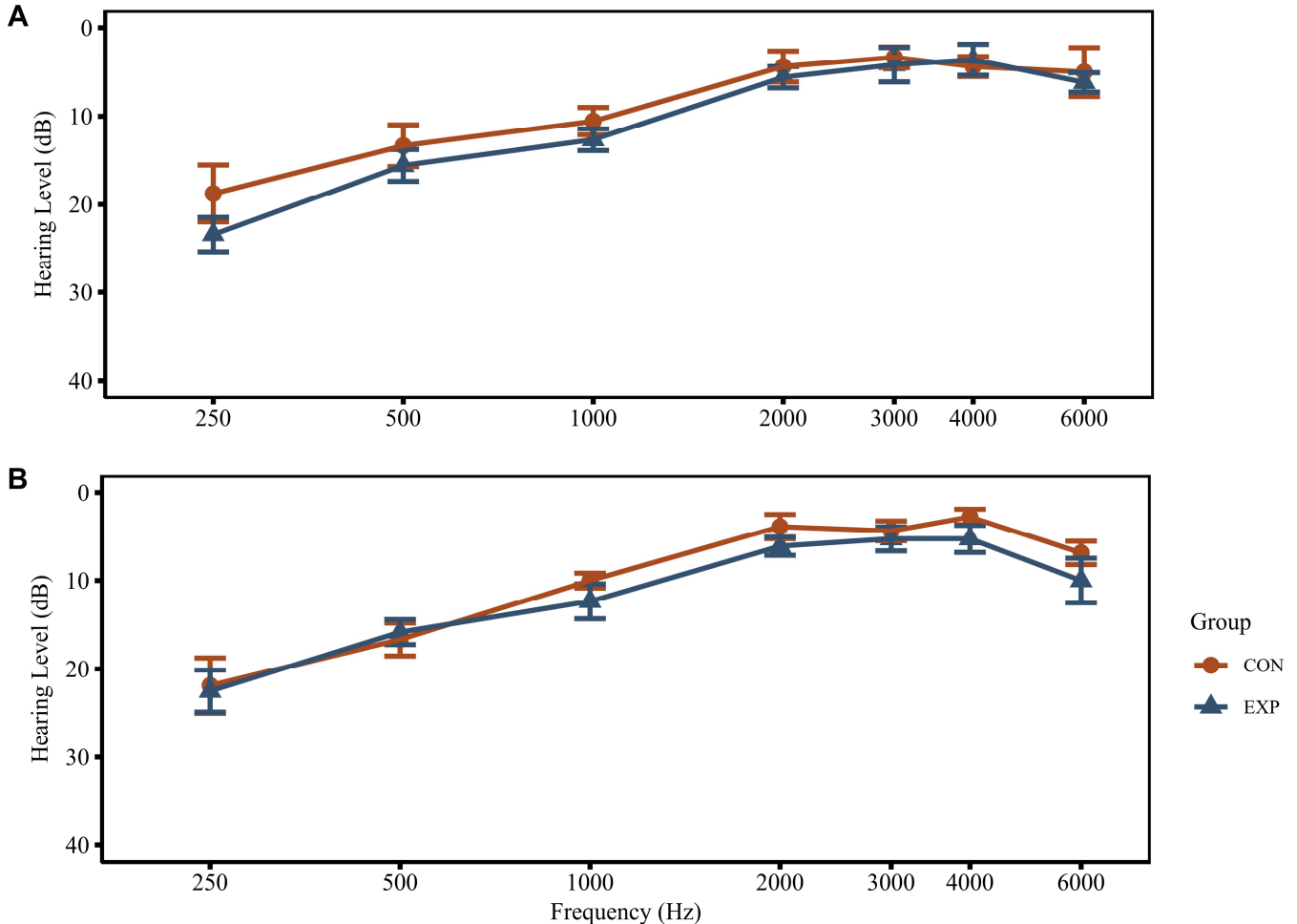
458 The interaction of group and session was assessed using a single unpaired approach. The change in CBF
459 between the session 1 pre-NT and session 5 post-NFT co-registered CBF maps were calculated for each
460 subject. Next, the statistical significance of the group differences in the change in CBF was determined using
461 permutation testing implemented using FSL randomise. Null t distributions for contrasts representative of the
462 interaction of session and group were derived by performing 1,000,000 random permutations and the
463 clustering method outlined above was implemented to account for false positives.

464 3. Results

465 3.1 Hearing Thresholds

466 Hearing thresholds were compared across groups for each frequency tested (250 Hz, 500 Hz, 1 kHz, 2 kHz, 3
467 kHz, 4 kHz, and 6 kHz) using Welch's t test. To be most conservative in the detection of a potential group
468 difference, no correction for multiple comparisons was applied. There were no observed significant
469 differences ($p > 0.05$, two-tailed) for any of the testing frequencies signifying the two groups had equivalent
470 hearing thresholds between 250 Hz and 6 kHz. It is important to note, the transducers utilized in this test

471 were calibrated but were not noise-attenuating. Therefore, the measured hearing levels may appear greater in
 472 testing frequencies less than 2 kHz due to ambient noise (*e.g.*, HVAC noise) transversing the ear cups
 473 especially since a soundproof room was not utilized for testing.

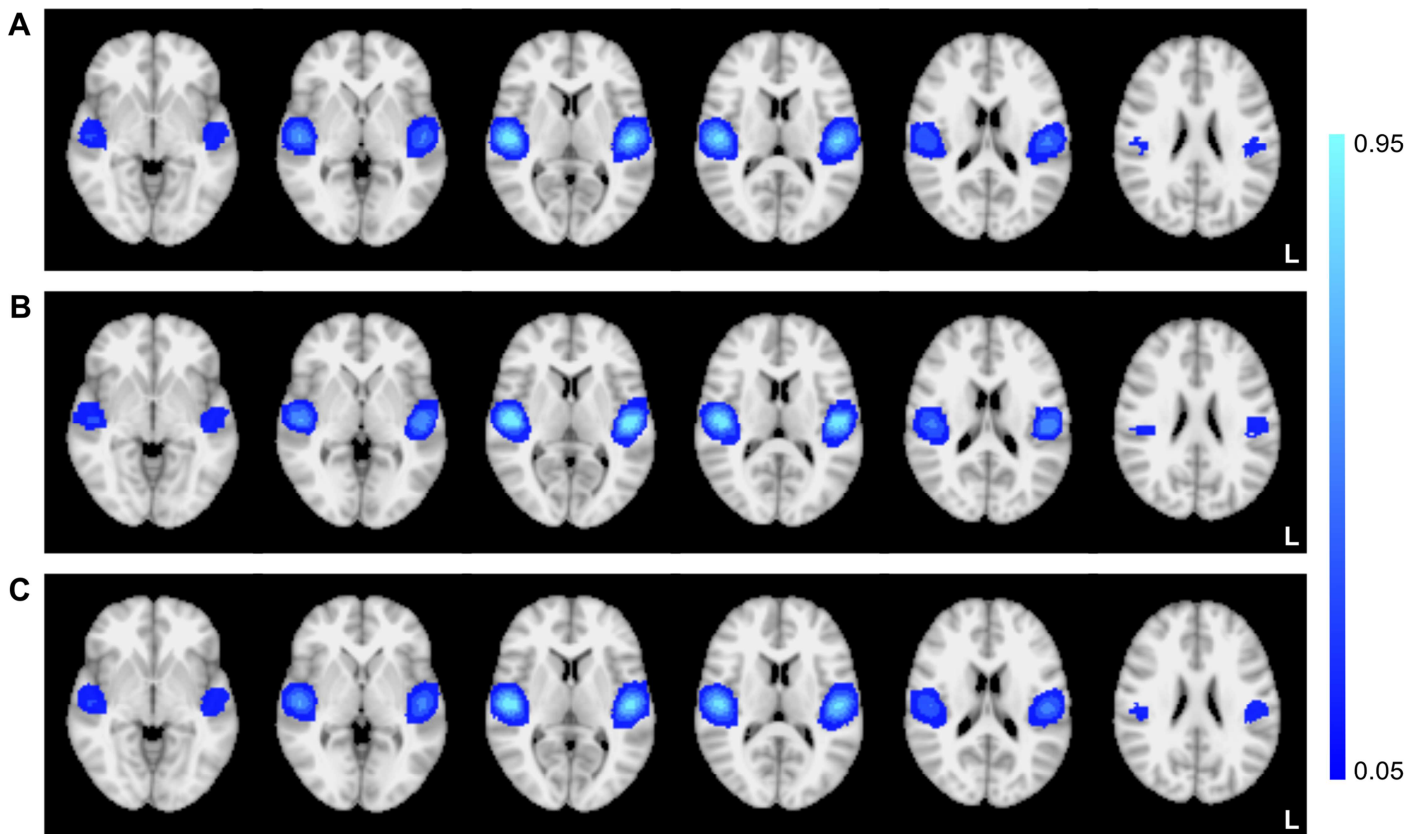


474

475 Figure 3. Audiogram results for the hearing levels of the (A) left and (B) right ear separated by group and
 476 frequency. No significant differences were observed between groups for all testing frequencies.

477 3.2 AC Control

478 A 2x5 repeated measures ANOVA evaluated the size of the functionally-defined AC VOI across sessions
 479 and groups (Figure 4). The size of the VOIs did not significantly differ between groups or sessions ($F_{1,100} =$
 480 0.208 , $p = 0.208$ and $F_{4,100} = 0.740$, $p = 0.567$, respectively, two-tailed). Furthermore, the interaction of
 481 session by group was not significant in the VOI size ($F_{4,100} = 0.531$, $p = 0.713$, two-tailed). Although the
 482 VOIs for the CON group were not used during neurofeedback, these VOIs were utilized for post-processing
 483 to compute AC de-activation. The average size of each VOI across groups and sessions was $1490 \text{ mm}^3 \pm$
 484 283.15 mm^3 .

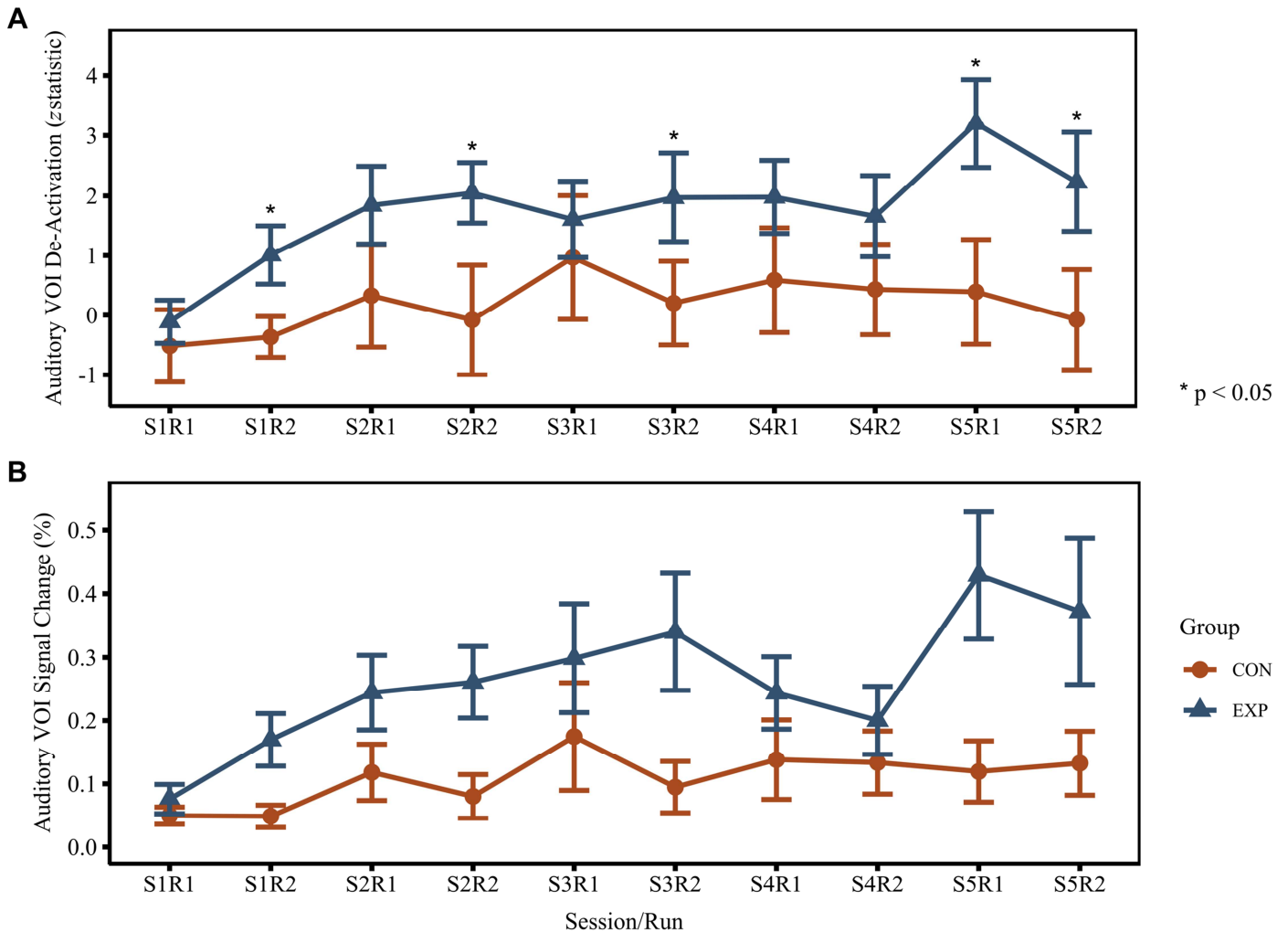


485
486

487 Figure 4. The probability of voxel inclusion during fMRI-NFT for (A) both EXP and CON groups, (B) EXP
488 group only, (C) CON group only. VOIs were transformed to standard space using the same transformation
489 responsible for morphing the fMRI data to standard space. Axial slices are displayed at MNI coordinates $z =$
490 $-6, 0, 8, 12, 18,$ and 24 mm (left to right).

491 A $5 \times 2 \times 2$ repeated measures ANOVA evaluated the effects of session, run, and group on AC de-activation
492 during closed-loop neuromodulation (Figure 5A). AC de-activation is representative of an individual's
493 ability to volitionally down-regulate the AC (*i.e.*, AC control). The results of the between-subjects effect
494 revealed a significant main effect of group ($F_{1,25} = 3.941, p = 0.029$, one-tailed). One-tailed statistics are
495 reported as the *a priori* hypothesis was that AC control would be greater in the EXP group. Mauchly's test
496 of sphericity was not significant for session ($p = 0.160$, two-tailed) or session by run interaction ($p = 0.776$,
497 two-tailed). These results validate the assumption of sphericity, which was used to assess the results of the
498 within-subjects tests henceforth. The results of the within-subjects testing identified a significant main effect
499 of session ($F_{4,100} = 2.702, p = 0.0175$, one-tailed). One-tailed statistics are reported as our *a priori* hypothesis
500 was that AC control would increase with training. The main effect of run was not significant ($F_{1,25} = 0.338,$
501 0.283 , one-tailed) along with the interaction effects of session by group ($F_{4,100} = 0.930, p = 0.225$, one-
502 tailed), run by group ($F_{1,25} = 0.908, p = 0.175$, one-tailed), session by run ($F_{4,100} = 1.772, p = 0.07$, one-
503 tailed), and session by run by group ($F_{4,100} = 0.953, p = 0.219$, one-tailed). *Post hoc*, Bonferroni-corrected
504 pairwise comparisons were conducted on the session by group interaction to evaluate differences between
505 sessions 2, 3, 4, and 5 with session 1. These results revealed there were significant differences between
506 sessions 5 ($p = 0.006$, one-tailed) and 2 ($p = 0.015$, one-tailed) in the EXP group while the remaining two
507 sessions (2 and 3) were close to significant ($p = 0.0528$ and $p = 0.0502$, respectively). For the CON group, no
508 comparison was near significant ($p > 0.4$ for all comparisons). Welch's *t* test were conducted between the

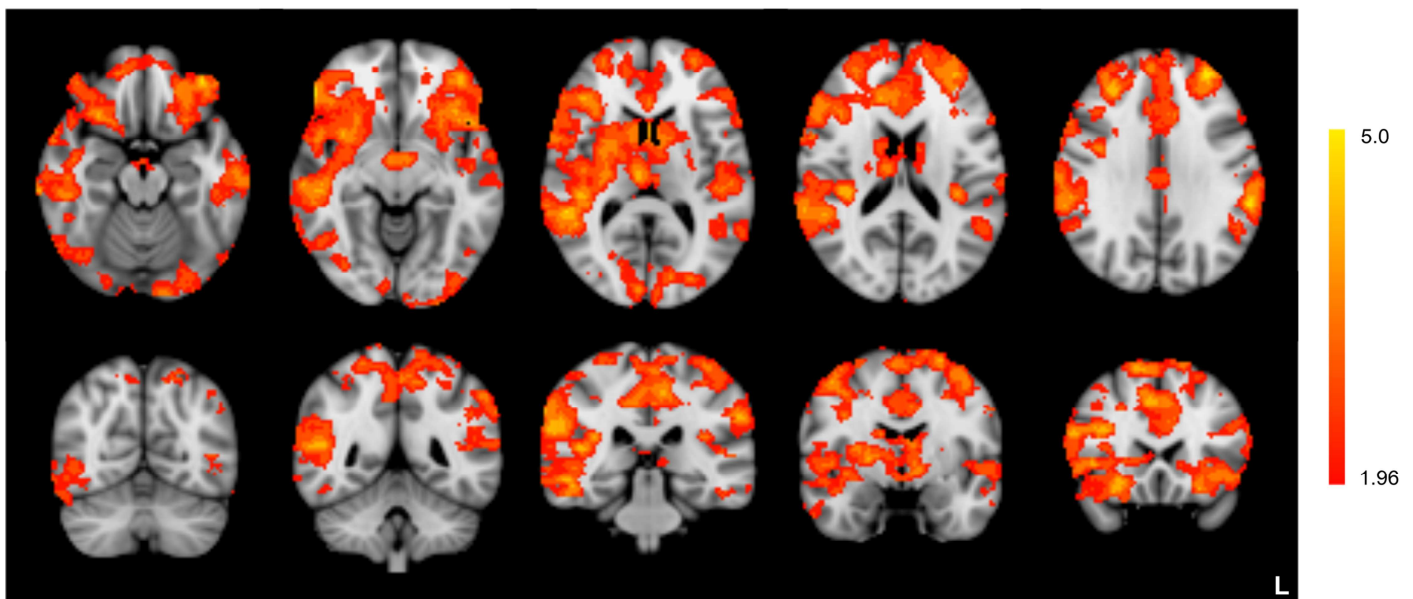
509 groups for each session/run. The EXP group had significantly greater AC control than the CON group for
 510 session 1 run 2 ($p = 0.015$, one-tailed), session 2 run 2 ($p = 0.0385$, one-tailed), session 3 run 2 ($p = 0.048$,
 511 one-tailed), session 5 run 1 ($p = 0.012$, one-tailed), and session 5 run 2 ($p = 0.0315$, one-tailed). For
 512 reference, the percent signal changes in the auditory VOI (Figure 5B) are presented along with the auditory
 513 VOI de-activation values.



514

515 Figure 5. Results from the AC VOI across all sessions and runs. VOI de-activation (A) and signal change (B)
 516 separated by group, session, and run.

517 A voxel-based 2x2 (group by session) repeated measures ANOVA was performed using FSL. The F test
 518 revealed a significant ($z > 1.96$) main effect of session on de-activation magnitude during neurofeedback in
 519 several regions throughout the brain, including bilateral changes in AC (Figure 6). It is important to note that
 520 we cannot identify which regions had stronger de-activation during neurofeedback in the fifth session than
 521 the first due to the bi-directionality of the F test. The contrasts identifying voxels with significantly greater
 522 activation and de-activation in session 5 than session 1 were assessed to clarify the directionality. We
 523 observed all of these regions in the de-activation contrast, implying directionality towards stronger de-
 524 activation in the fifth neurofeedback session, which supports the results of the VOI analysis.

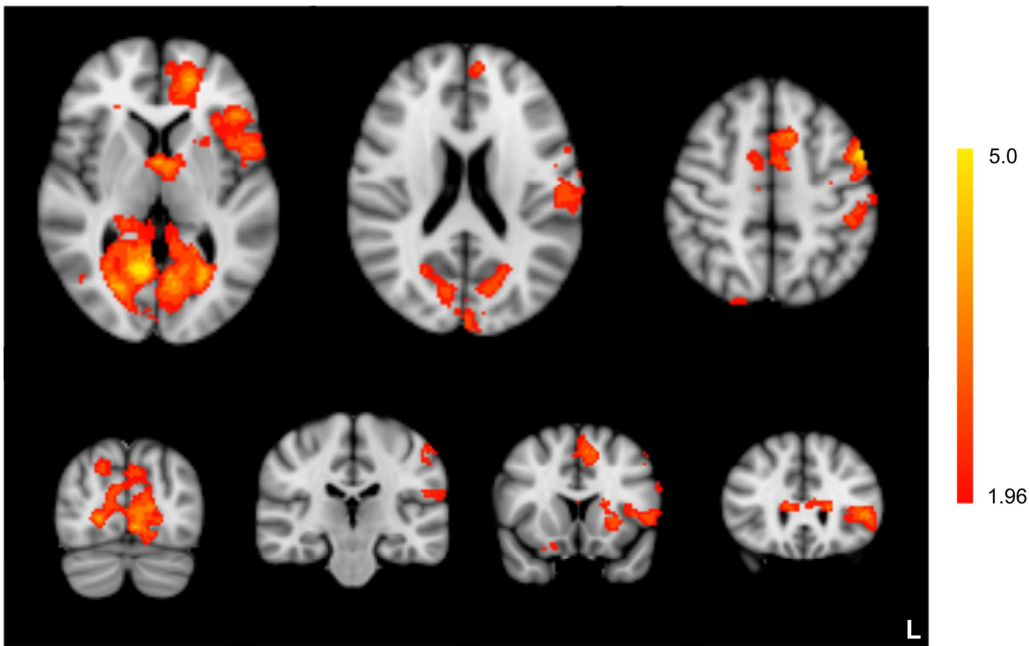


525

526 Figure 6. F test results for the main effect of session indicate increased de-activation during neurofeedback
 527 across training for several brain regions. Axial slices (top row) are displayed at MNI coordinates $z = -18, -8,$
 528 $10, 18,$ and 30 mm (left to right). Coronal slices (bottom row) are displayed at MNI coordinates $y = -64, -48,$
 529 $-32, -4,$ and 20 mm (left to right).

530

531 Additionally, the F test revealed a significant ($z > 1.96$) interaction of session by group on de-activation
 532 during neurofeedback (Figure 7). Bilateral changes were found in the thalamus, lingual gyrus, and the
 533 cuneus. Changes in the superior frontal gyrus, medial frontal gyrus, inferior frontal gyrus, precentral gyrus,
 534 and postcentral gyrus only appeared in the left hemisphere. In *post hoc* comparisons, a few small regions
 535 were significantly more de-activated in the EXP group than the CON group during session 1 with local
 536 maxima appearing in the right middle frontal gyrus and the left fusiform (Figure 8A). The bilateral auditory
 537 cortex appeared in the contrast identifying voxels significantly more de-activated in the EXP group at session
 538 5, along with local maxima in the right inferior frontal cortex, right middle frontal gyrus, and the left middle
 539 temporal gyrus (Figure 8B). There were significant differences in de-activation between sessions 1 and 5 for
 540 the CON group in the auditory cortex as well as local maxima in the left middle frontal gyrus, bilateral
 541 superior frontal gyrus, and left inferior parietal lobule (Figure 9A). The EXP group also shows significant
 542 differences in de-activation from session 1 to session 5 as the CON group, but to a larger magnitude and
 extent (Figure 9B).



543

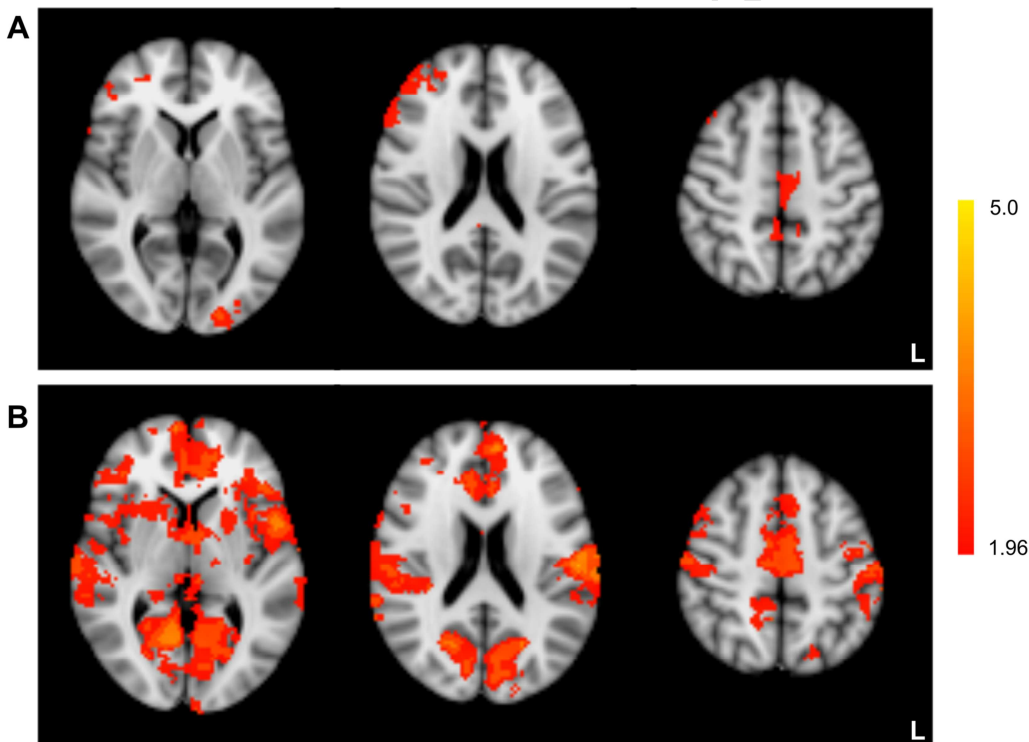
544

545

546

547

Figure 7. *F* test results for the interaction of session by group from closed-loop endogenous neuromodulation. Axial slices (top row) are displayed at MNI coordinates $z = 4, 20,$ and 50 mm (left to right). Coronal slices (bottom row) are displayed at MNI coordinates $y = -76, -24, 14,$ and 26 mm (left to right).



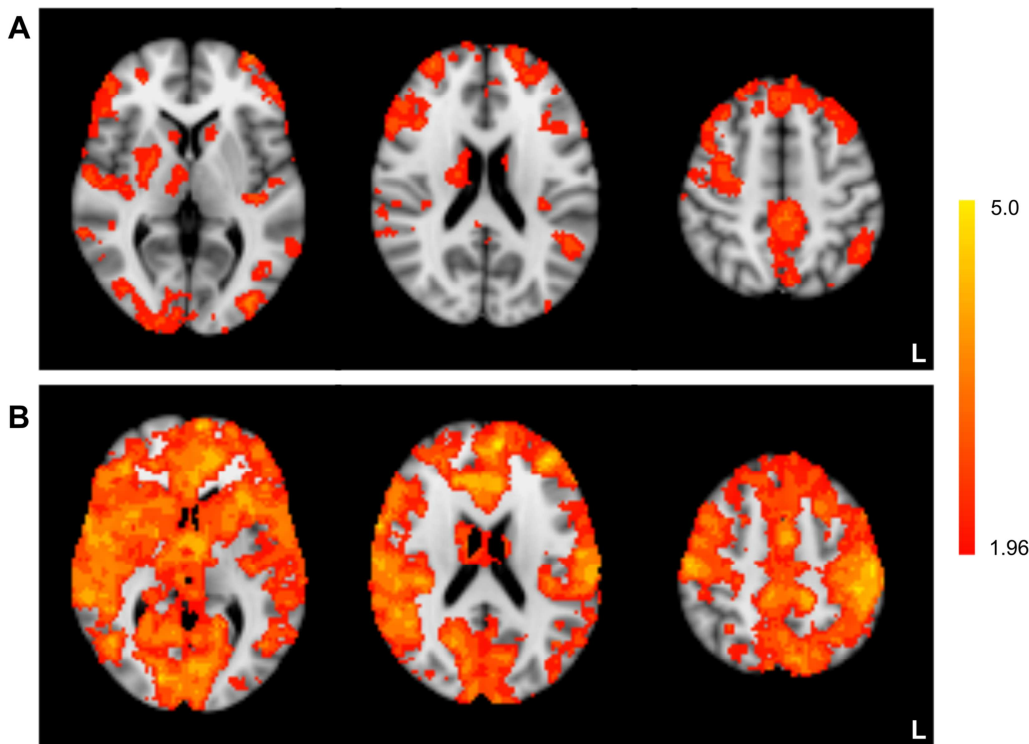
548

549

550

551

Figure 8. Contrast identifying increased de-activation in the EXP group compared to the CON group during closed-loop endogenous neuromodulation for sessions 1 (A) and 5 (B). Axial slices are displayed at MNI coordinates $z = 4, 20,$ and 50 mm (left to right).



552

553 Figure 9. Contrast identifying increased de-activation from session 1 to session 5 during closed-loop
 554 endogenous neuromodulation in the CON (A) and EXP (B) groups. Axial slices are displayed at MNI
 555 coordinates $z = 4, 20,$ and 50 mm (left to right).

556 3.3 Behavioral Assessment

557 The effects of group and session on ACS total score, a subjective measure of attentional control, were
 558 evaluated using a repeated-measures ANOVA. The between-subjects effects revealed the main effect of
 559 group was not significant ($F_{1,25} = 0.029, p > 0.05,$ one-tailed). The results of the within-subjects testing
 560 identified the main effect of session was not significant ($F_{1,25} = 0.01, p > 0.05,$ one-tailed). The interaction
 561 effect of session and group was not significant ($F_{1,25} = 0.104, p > 0.05,$), therefore no *post hoc* testing was
 562 performed.

563 A repeated measures ANOVA evaluated the effects of group and session on ΔAE mean latency. The results
 564 of the tests of between-subjects effects revealed the main effect of group was significant ($F_{1,25} = 3.267, p =$
 565 $0.042,$ one-tailed), with a greater distractibility in the EXP group on average. The within-subjects testing
 566 identified the main effect of session and the session by group interaction effect were not significant ($F_{1,25} =$
 567 $0.125, p = 0.364$ and $F_{1,25} = 0.012, p = 0.457,$ respectively).

568 The results of the 2×2 repeated measures ANOVA for CPT-X sensitivity (d') revealed the main effect of
 569 group was not significant ($F_{1,25} = 0.507, p = 0.242,$ one-tailed). The results of the within-subjects testing
 570 identified the main effect of session and the session by group interaction were not significant ($F_{1,25} = 1.095, p$
 571 $= 0.153$ and $F_{1,25} = 0.010, p = 0.461,$ respectively). One-tailed statistics are reported as our *a priori*
 572 hypothesis was that ACS total score and CPT-X sensitivity would increase with training and ΔAE mean
 573 latency would decrease with training, and these changes would be greater in the EXP group.

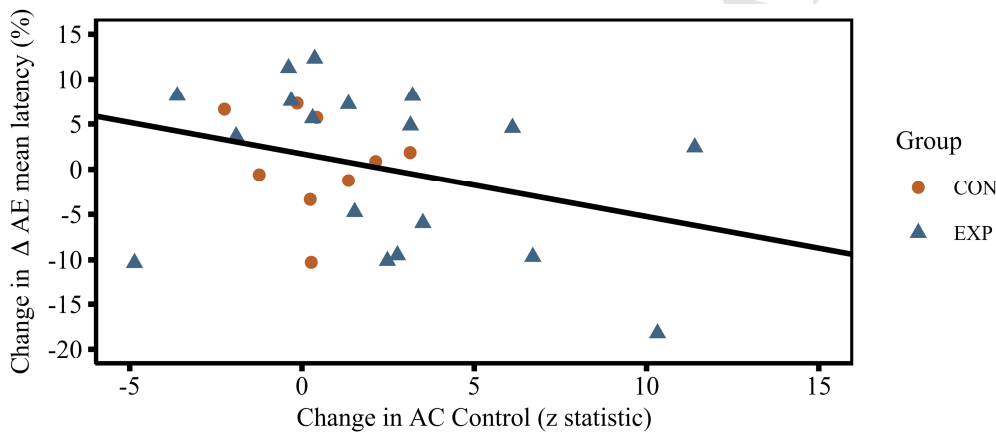
574 3.4 AC Control – Behavior Correlation

575 Changes across training in behavior (session 5 minus session 1) and AC control (session 5, run 2 minus
 576 session 1 run 1) were computed. Bivariate correlations (Table 1) were carried out in SPSS to evaluate the
 577 relationship between these changes in behavior and AC control under the hypothesis that those individuals
 578 with the greatest change in AC control will have more profound changes in behavior. The change in AC
 579 control was found to have a significant negative correlation with the change in Δ AE mean latency (Pearson's
 580 $r = -0.323$, $p = 0.05$). Separated by group, the correlation was not significant for either the CON group
 581 (Pearson's $r = -0.183$, $p = 0.318$) or the EXP group (Pearson's $r = -0.347$, $p = 0.079$). The change in ACS
 582 total score and CPT-X sensitivity were not significantly correlated to AC control in neither combined nor
 583 group-separated analyses.

584 Table 1. Results of the bivariate correlation analysis. Highlighted columns indicate significance at or below p
 585 $= 0.05$.

		ACS Total Score	CPT-X Sensitivity (d')	Δ AE Mean Latency (%)
AC control	Pearson's r	.244	.119	-.323
	Significance (one-tailed)	.110	.277	.050
	n	27	27	27

586



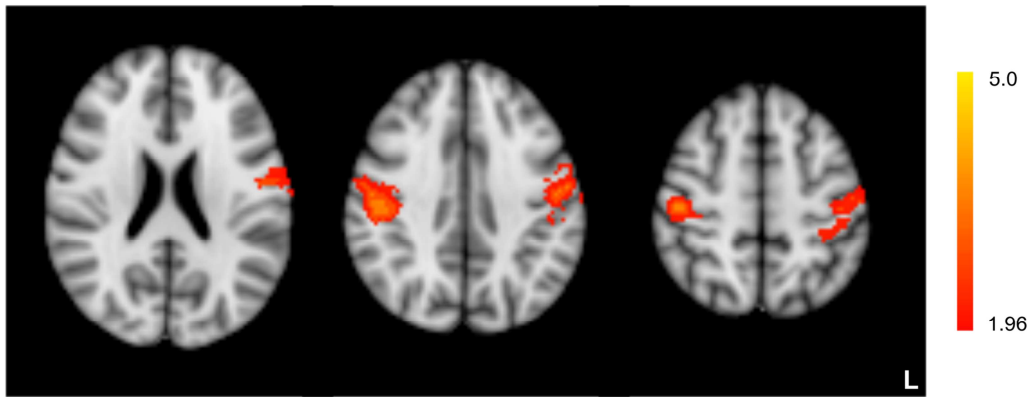
587

588 Figure 10. Bivariate correlation results. A significant negative relationship ($r = -0.323$, $p = 0.05$) between the
 589 change in AC control and the change in Δ AE mean latency was revealed.

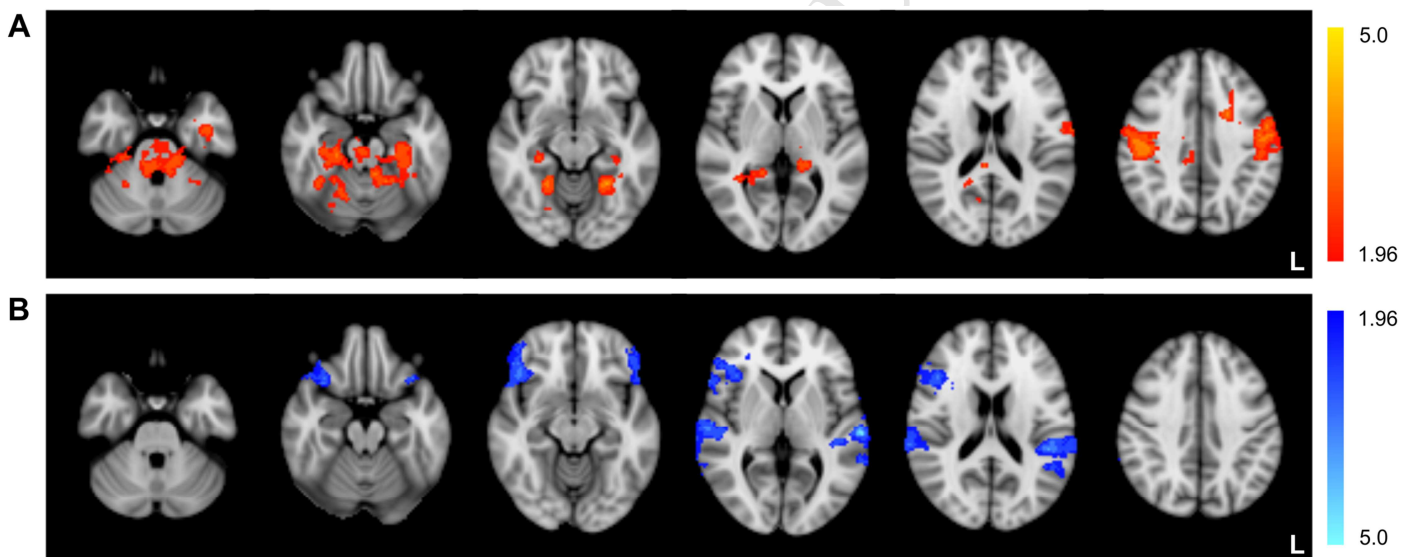
590 3.5 Binaural Auditory Stimulation

591 A 2x2 (group by session) repeated measures ANOVA was performed using FSL. The F test revealed a
 592 significant ($z > 1.96$) main effect of session on activation magnitude during binaural auditory stimulation
 593 bilaterally in the precentral and postcentral gyri (Figure 11). It is important to note that we cannot identify
 594 which regions had stronger activation or de-activation due to the bi-directionality of the F test, and whether
 595 this increased or decreased from session 1 to session 5. The contrasts identifying voxels with significantly
 596 greater activation and de-activation in session 5 than session 1 were assessed separately to clarify the
 597 directionality. We observed both the precentral and postcentral gyrus in the activation contrast, implying
 598 directionality towards stronger activation in the fifth session (Figure 12A). The contrast identifying voxels
 599 less activated on session 5 than session 1 (or greater de-activation) revealed a significant effect in the right

600 inferior frontal gyrus and bilateral auditory cortex (Figure 12B). The F test did not reveal any significant
 601 findings for the interaction of session by group on activation during binaural auditory stimulation.



602
 603 Figure 11. F test results for the main effect of session indicate increased activation in the precentral and
 604 postcentral gyri across training in response to binaural auditory stimulation. Axial slices are displayed at
 605 MNI coordinates $z = 22, 38, \text{ and } 52$ mm (left to right).



606
 607 Figure 12. Contrast identifying voxels with significantly increased (A) and decreased (B) activation across
 608 training in response to binaural auditory stimulation. Axial slices are displayed at MNI coordinates $z = -30, -$
 609 $20, -12, 4, 18, \text{ and } 38$ mm (left to right).

610 3.6 Steady-State Perfusion

611 Permutation testing was conducted to evaluate the main effect of session and the interaction between session
 612 and group using two-sample paired and unpaired testing, respectively. A main effect of session was found in
 613 a few small clusters and are most likely false positives. The unpaired testing revealed a significantly larger
 614 change in CBF in the EXP group compared with the CON group in several regions: bilateral inferior parietal
 615 lobule, the left inferior frontal gyrus, superior parietal lobule, middle temporal gyrus, ACC and precentral
 616 gyrus, as well as the right fusiform gyrus (Figure 13).

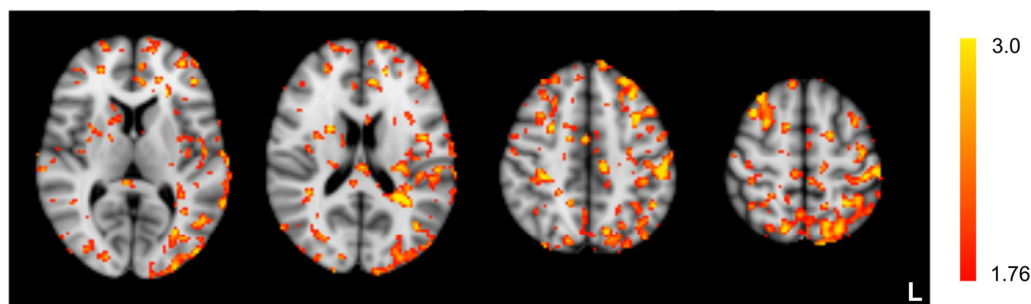


Figure 13. Differential changes in cerebral perfusion across fMRI-NFT between groups. Axial slices are displayed at MNI coordinates $z = 8, 18, 46,$ and 56 mm (left to right).

4. Discussion

The study presented in this work trained down-regulation of the auditory cortex using fMRI-NFT and directed attention strategies. Such a technique may be applicable to the treatment of neurologic disorders such as tinnitus. The experimental group attempted self-regulation with the aid of real information regarding the current BOLD signals in the AC while the control group was supplied sham feedback yoked from a random participant in the experimental group and matched for training progress. In both groups, the bilateral AC was identified both anatomically and functionally using an activation map produced during binaural continuous noise stimulation at each of the five training sessions. The results indicate an overall increase in the ability to volitionally decrease AC activity across training, a region known to be hyperactive in chronic tinnitus. Activation changes in other regions during closed-loop endogenous neuromodulation were also observed much of the frontal cortex, and anterior cingulate indicating the involvement of attentional and monitoring processes. The frontal cortex and anterior cingulate are likely involved with auditory attention processes (Roberts et al., 2013). Control over AC de-activation was not found to be significantly different at the first session between the experimental and control groups. However, the ability to volitionally decrease AC activity was observed to be significantly greater for the experimental group compared to the control group at sessions two and five. Furthermore, self-control over AC de-activation between the first and last training session was significantly increased in the experimental group. There was also a significant increase between the first and second training session signifying a rapid effect of neurofeedback training on AC control. These effects were not observed in the control group.

These results add to a growing body of research that demonstrates the success of fMRI-NFT in teaching individuals to self-regulate localized brain activity. A previous controlled study indicates healthy individuals can learn to control the activated cortical volume in the primary and secondary auditory cortex using fMRI-NFT (Yoo et al., 2006). A second previous study indicated that control over the magnitude of A1 activation is also achievable however not necessarily attributable to fMRI-NFT (Haller et al., 2010). A third previous study implication the possibility of tinnitus patients to down-regulate the auditory cortex using continuous and intermittent neurofeedback (Emmert et al., 2017a). Single-session results identified greater down-regulation in the intermittent feedback group; but over multiple sessions, the continuous feedback was more advantageous. The results above support the previous finding that fMRI-NFT aids control over the magnitude of AC de-activation, and this capability can be trained in the presence of sound. Moreover, this result shows that 60 min of distributed fMRI-NFT is adequate to train AC self-regulation, but significant observable effects are prevalent within 24 min of training.

Training self-regulation of brain activity from fMRI-NFT has shown promise in a broad range of applications such as the improvement of human performance (Scharnowski et al., 2012; Sherwood et al., 2016a; Zhang et al., 2013) and a variety of medical applications including recovery from stroke (Chiew et

654 al., 2012; Liew et al., 2016), major depression (Linden et al., 2012; Mehler et al., 2018; Young et al., 2014;
655 Yuan et al., 2014), Parkinson's disease (Subramanian et al., 2011), and chronic pain (deCharms et al., 2005;
656 Emmert et al., 2017b; Zhang et al., 2018). However, only a few previous studies have investigated fMRI-
657 NFT as a possible treatment for tinnitus (Emmert et al., 2017a; Haller et al., 2010; Yoo et al., 2006).

658 Moreover, this work evaluated the neural and behavioral implications by assessing the impact of fMRI-NFT
659 on attentional processes. The results of the work presented herein do suggest improved control over the
660 activity of the AC did lead to decreased distractibility (*i.e.*, increased attentional control), a result that did not
661 survive when the groups were separated. This finding implies that attempting volitional down-regulation of
662 the AC may alter distractibility and attentional control. This research also measured changes in neural
663 processes associated with fMRI-NFT. The results of this work identified a significant reduction in AC
664 activity in response to binaural continuous noise stimulation. Due to this effect being prevalent across both
665 experimental and control groups, it may be a training effect or stimulus adaptation; however, it is also
666 plausible that this effect is from attempted down-regulation of auditory activity. Unfortunately, this research
667 lacks the ability to differentiate these effects. It should be noted that our use of a task-based white noise
668 paradigm with continuous scanning may not have been optimal for mapping of the AC, and this may have
669 impacted our ability to find an interaction effect in the AC localization procedure across sessions. Our design
670 was chosen to keep the fMRI and NFT sequences as similar as possible and to minimize differences in AC
671 response associated with individual tonal-specific hearing differences, which were not controlled.

672 Similarly, differential changes in resting cerebral perfusion were observed across training between the
673 groups. Due to the infancy of ASL and that it has yet to be clearly quantitatively validated, these findings
674 should be interpreted cautiously. Xu et al. (2010) found a high reliability of perfusion measures in 3D pcASL
675 measurements of perfusion in both young and older subjects. Further, they found agreement between
676 measurements of perfusion between 3D pcASL and ¹⁵O-water positron emission tomography in older
677 individuals. However, we have implemented ASL in the methodology set forth by Alsop et al. (2015) which
678 describes the optimal default implementation for clinical applications resulting from a consensus of the
679 ISMRM Perfusion Study Group that was reached in October 2012.

680 Finally, this study has many limitations which may impact the interpretation of the findings. First and
681 foremost, the differential sample sizes between our control ($n = 9$) and experimental ($n = 18$) groups.
682 Unequal sample sizes can affect the homogeneity of variance assumptions and power. Due to power being
683 computed from the smallest sample size, the disproportionate grouping should have decreased our ability to
684 observe significant effects between the experimental and control groups. Despite this, there were significant
685 effects observed in several measures. The unequal groups was part of our design to make best use of the
686 project funds while accounting for future portions of the funded effort. Another limitation is that our
687 participants were healthy. While our funding and effort is focused on tinnitus, this particular study was really
688 focused on utilizing an existing fMRI-NFT paradigm (left prefrontal cortex) to see if activity of a different
689 brain region (auditory cortex) can be down-regulated while concurrently providing auditory stimulation.
690 With deactivation of a new brain region being the main focus, other measures (*e.g.*, behavioral) were
691 secondary and could have been more robustly developed and applied. However, to reiterate, our goal was to
692 show that our neurofeedback approach successfully enabled participants to control activity in their auditory
693 cortex. This region and down-regulation were specifically chosen due to the hyperactivity of the auditory
694 cortex that has been associated with tinnitus patients (Gu et al., 2010; Langguth et al., 2006; Schecklmann et
695 al., 2013; Seydell-Greenwald et al., 2012; Wang et al., 2001). A third limitation was the single-blinded
696 nature of this study where only the participants were blinded to the grouping. Originally, we designed the
697 control condition differently and in such a way that double-blinding was not possible. After piloting, we
698 determined this method was flawed and implemented the method presented in this paper without adding
699 blinding to the researchers. Single-blinded studies may cause researchers to inadvertently place unequal

700 demand characteristics on the groups leading to downstream differences in behavior and brain activity
701 (Thibault et al., 2018). A further limitation is the absence of accounting for respiration artifacts (*e.g.*,
702 respiration volume and heart rate variability) which can significantly alter the BOLD signal or provide the
703 experimental group, but not control group, with a form of respiration biofeedback that may help them
704 achieve self-regulation (Thibault et al., 2018).

705 **5. Conclusion**

706 The results presented in this work align with previous findings which indicate fMRI-NFT can teach control
707 over the auditory cortex. However, the results of the presented work add to the previous findings by
708 indicating volitional down-regulation of the auditory cortex is achievable using fMRI-NFT, and that this
709 control is possible in the presence of continuous noise. Our findings suggest future work should evaluate the
710 efficacy of attempting down-regulation of the auditory cortex in the presence of binaural auditory stimulation
711 in a cohort of tinnitus patients. Tinnitus is a neurologic disorder associated with hyperactivity of the auditory
712 cortex and reduced attentional control leading to increased attention directed towards the auditory system.
713 This is exacerbated by enhanced emotional responses to auditory stimuli. Tinnitus can cause severe
714 impairments and may even limit the ability to perform daily functions. The number of U.S. veterans
715 receiving service-connected disability compensation for tinnitus exceeds all other compensation recipient
716 disabilities including post-traumatic stress disorder, hearing loss, and lumbosacral or cervical strain.
717 Although this work demonstrated fMRI-NFT aided the ability to control the auditory cortex, the findings
718 were not limited to the group which received real neurofeedback. These findings represent the possibility of
719 such a treatment to be transitioned outside of the MRI to possible home-based therapies which may be
720 provided through mobile applications or simple to use devices.

721 **6. Acknowledgements**

722 This material is based on research sponsored by the U.S. Air Force under agreement number FA8650-16-2-
723 6702. The views expressed are those of the authors and do not reflect the official views or policy of the
724 Department of Defense and its Components. The U.S. Government is authorized to reproduce and distribute
725 reprints for Governmental purposes notwithstanding any copyright notation thereon. The voluntary, fully
726 informed consent of the subjects used in this research was obtained as required by 32 CFR 219 and DODI
727 3216.02_AFI 40-402.

728 **7. Conflict of Interest**

729 The authors declare that this research was conducted in the absence of any commercial or financial
730 relationships that could be construed as a potential conflict of interest.

731 **8. References**

- 732 Alsop, D.C., Detre, J.A., 1996. Reduced Transit-Time Sensitivity in Noninvasive Magnetic Resonance
733 Imaging of Human Cerebral Blood Flow. *J. Cereb. Blood Flow Metab.* 16, 1236–1249.
734 <https://doi.org/10.1097/00004647-199611000-00019>
- 735 Alsop, D.C., Detre, J.A., Golay, X., Günther, M., Hendrikse, J., Hernandez-Garcia, L., Lu, H., MacIntosh,
736 B.J., Parkes, L.M., Smits, M., van Osch, M.J.P., Wang, D.J.J., Wong, E.C., Zaharchuk, G., 2015.
737 Recommended implementation of arterial spin-labeled perfusion MRI for clinical applications: A
738 consensus of the ISMRM perfusion study group and the European consortium for ASL in dementia.
739 *Magn. Reson. Med.* 73, 102–116. <https://doi.org/10.1002/mrm.25197>
- 740 Anderson, M.J., Robinson, J., 2001. Permutation tests for linear models. *Aust. N. Z. J. Stat.* 43, 75–88.

- 741 <https://doi.org/10.1111/1467-842X.00156>
- 742 Ashby, F.G., 2011. Statistical analysis of fMRI data. MIT press.
- 743 Caria, A., Veit, R., Sitaram, R., Lotze, M., Weiskopf, N., Grodd, W., Birbaumer, N., 2007. Regulation of
744 anterior insular cortex activity using real-time fMRI. *NeuroImage* 35, 1238–1246.
745 <https://doi.org/10.1016/j.neuroImage.2007.01.018>
- 746 Chen, W.J., Hsiao, C.K., Hsiao, L.-L., Hwu, H.-G., 1998. Performance of the Continuous Performance Test
747 among community samples. *Schizophr. Bull.* <https://doi.org/10.1093/oxfordjournals.schbul.a033308>
- 748 Chiew, M., LaConte, S.M., Graham, S.J., 2012. Investigation of fMRI neurofeedback of differential primary
749 motor cortex activity using kinesthetic motor imagery. *NeuroImage* 61, 21–31.
750 <https://doi.org/http://dx.doi.org/10.1016/j.neuroImage.2012.02.053>
- 751 Collins, D.L., Holmes, C.J., Peters, T.M., Evans, A.C., 1995. Automatic 3-D model-based neuroanatomical
752 segmentation. *Hum. Brain Mapp.* 3, 190–208. <https://doi.org/10.1002/hbm.460030304>
- 753 Cox, R.W., Jesmanowicz, A., Hyde, J.S., 1995. Real-Time Functional Magnetic Resonance Imaging. *Magn.*
754 *Reson. Med.* 33, 230–236. <https://doi.org/10.1002/mrm.1910330213>
- 755 deCharms, R.C., Maeda, F., Glover, G.H., Ludlow, D., Pauly, J.M., Soneji, D., Gabrieli, J.D.E., Mackey,
756 S.C., 2005. Control over brain activation and pain learned by using real-time functional MRI. *Proc.*
757 *Natl. Acad. Sci. U. S. A.* 102, 18626–18631. <https://doi.org/10.1073/pnas.0505210102>
- 758 Derryberry, D., Reed, M.A., 2002. Anxiety-related attentional biases and their regulation by attentional
759 control. *J. Abnorm. Psychol.* <https://doi.org/10.1037/0021-843X.111.2.225>
- 760 Dixon, W.T., Sardashti, M., Castillo, M., Stomp, G.P., 1991. Multiple inversion recovery reduces static
761 tissue signal in angiograms. *Magn. Reson. Med.* 18, 257–268. <https://doi.org/10.1002/mrm.1910180202>
- 762 Emmert, K., Kopel, R., Koush, Y., Maire, R., Senn, P., Van De Ville, D., Haller, S., 2017. Continuous vs.
763 Intermittent Neurofeedback to Regulate Auditory Cortex Activity of Tinnitus Patients Using Real-Time
764 fMRI – A Pilot Study. *NeuroImage Clin.* 14, 97–104. <https://doi.org/10.1016/j.nicl.2016.12.023>
- 765 Emmert, K., Breimhorst, M., Bauermann, T., Birklein, F., Rebhorn, C., Van De Ville, D., Haller, S., 2017.
766 Active pain coping is associated with the response in real-time fMRI neurofeedback during pain. *Brain*
767 *Imaging Behav.* 11(3), 712–721. <https://doi.org/10.1007/s11682-016-9547-0>
- 768 Fera, F., Yongbi, M.N., van Gelderen, P., Frank, J.A., Mattay, V.S., Duyn, J.H., 2003. EPI-BOLD fMRI of
769 human motor cortex at 1.5 T and 3.0 T: Sensitivity dependence on echo time and acquisition bandwidth.
770 *J. Magn. Reson. Imaging* 19, 19–26. <https://doi.org/10.1002/jmri.10440>
- 771 Folmer, R.L., Theodoroff, S.M., Martin, W.H., Shi, Y., 2014. Experimental, Controversial, and Futuristic
772 Treatments for Chronic Tinnitus. *J. Am. Acad. Audiol.* 25, 106–125. <https://doi.org/10.3766/jaaa.25.1.7>
- 773 Friston, K.J., Holmes, A.P., Poline, J.-B., Grasby, P.J., Williams, S.C.R., Frackowiak, R.S.J., Turner, R.,
774 1995. Analysis of fMRI Time-Series Revisited. *NeuroImage* 2, 45–53. <https://doi.org/10.1006/nimg.1995.1007>
- 775
- 776 Glover, G.H., 2012. Spiral imaging in fMRI. *NeuroImage* 62, 706–712.
777 <https://doi.org/10.1016/J.NEUROIMAGE.2011.10.039>
- 778 Green, D.M., Swets, J.A., 1966. Signal Detection Theory and Psychophysics. Wiley, New York, NY.
- 779 Greve, D.N., Fischl, B., 2009. Accurate and robust brain image alignment using boundary-based registration.
780 *NeuroImage* 48, 63–72. <https://doi.org/10.1016/j.neuroImage.2009.06.060>

- 781 Gu, J.W., Halpin, C.F., Nam, E.-C., Levine, R.A., Melcher, J.R., 2010. Tinnitus, Diminished Sound-Level
782 Tolerance, and Elevated Auditory Activity in Humans With Clinically Normal Hearing Sensitivity. *J.*
783 *Neurophysiol.* 104, 3361–3370.
- 784 Halford, J.B.S., Anderson, S.D., 1991. Anxiety and depression in tinnitus sufferers. *J. Psychosom. Res.* 35,
785 383–390. [https://doi.org/10.1016/0022-3999\(91\)90033-K](https://doi.org/10.1016/0022-3999(91)90033-K)
- 786 Haller, S., Birbaumer, N., Veit, R., 2010. Real-time fMRI feedback training may improve chronic tinnitus.
787 *Eur. Radiol.* 20, 696–703. <https://doi.org/10.1007/s00330-009-1595-z>
- 788 Hamilton, J.P., Glover, G.H., Hsu, J.-J., Johnson, R.F., Gotlib, I.H., 2011. Modulation of subgenual anterior
789 cingulate cortex activity with real-time neurofeedback. *Hum. Brain Mapp.* 32, 22–31.
790 <https://doi.org/10.1002/hbm.20997>
- 791 Harris, C.R., Pashler, H., 2004. Attention and the Processing of Emotional Words and Names: Not So
792 Special After All. *Psychol. Sci.* 15, 171–178. <https://doi.org/10.1111/j.0956-7976.2004.01503005.x>
- 793 Hyde, J.S., Biswal, B.B., Jesmanowicz, A., 2001. High-resolution fMRI using multislice partial k-space GR-
794 EPI with cubic voxels. *Magn. Reson. Med.* 46, 114–125. <https://doi.org/10.1002/mrm.1166>
- 795 Jenkinson, M., Bannister, P., Brady, M., Smith, S., 2002. Improved Optimization for the Robust and
796 Accurate Linear Registration and Motion Correction of Brain Images. *NeuroImage* 17, 825–841.
797 <https://doi.org/10.1006/nimg.2002.1132>
- 798 Jenkinson, M., Smith, S., 2001. A global optimisation method for robust affine registration of brain images.
799 *Med. Image Anal.* 5, 143–156. [https://doi.org/10.1016/S1361-8415\(01\)00036-6](https://doi.org/10.1016/S1361-8415(01)00036-6)
- 800 Johnston, S., Linden, D.E.J., Healy, D., Goebel, R., Habes, I., Boehm, S.G., 2011. Upregulation of emotion
801 areas through neurofeedback with a focus on positive mood. *Cogn. Affect. Behav. Neurosci.* 11, 44–51.
802 <https://doi.org/10.3758/s13415-010-0010-1>
- 803 Jun, H.J., Park, M.K., 2013. Cognitive Behavioral Therapy for Tinnitus: Evidence and Efficacy. *Korean J.*
804 *Audiol.* 17, 101–104. <https://doi.org/10.7874/kja.2013.17.3.101>
- 805 Langers, D.R.M., Krumbholz, K., Bowtell, R.W., Hall, D.A., 2014a. Neuroimaging paradigms for tonotopic
806 mapping (I): The influence of sound stimulus type. *Neuroimage* 100, 650–662.
807 <https://doi.org/10.1016/J.NEUROIMAGE.2014.07.044>
- 808 Langers, D.R.M., Sanchez-Panchuelo, R.M., Francis, S.T., Krumbholz, K., Hall, D.A., 2014b. Neuroimaging
809 paradigms for tonotopic mapping (II): The influence of acquisition protocol. *Neuroimage* 100, 663–675.
810 <https://doi.org/10.1016/J.NEUROIMAGE.2014.07.042>
- 811 Langers, D.R.M., van Dijk, P., 2011. Robustness of intrinsic connectivity networks in the human brain to the
812 presence of acoustic scanner noise. *Neuroimage* 55, 1617–1632.
813 <https://doi.org/10.1016/J.NEUROIMAGE.2011.01.019>
- 814 Langguth, B., Eichhammer, P., Kreutzer, A., Maenner, P., Marienhagen, J., Kleinjung, T., Sand, P., Hajak,
815 G., 2006. The impact of auditory cortex activity on characterizing and treating patients with chronic
816 tinnitus – first results from a PET study. *Acta Otolaryngol.* 126, 84–88.
817 <https://doi.org/10.1080/03655230600895317>
- 818 Liew, S.-L., Rana, M., Cornelsen, S., Fortunato de Barros Filho, M., Birbaumer, N., Sitaram, R., Cohen,
819 L.G., Soekadar, S.R., 2015. Improving Motor Corticothalamic Communication After Stroke Using
820 Real-Time fMRI Connectivity-Based Neurofeedback. *Neurorehabil. Neural Repair* 30, 671–675.
821 <https://doi.org/10.1177/1545968315619699>

- 822 Linden, D.E.J., Habes, I., Johnston, S.J., Linden, S., Tatineni, R., Subramanian, L., Sorger, B., Healy, D.,
823 Goebel, R., 2012. Real-Time Self-Regulation of Emotion Networks in Patients with Depression. *PLoS*
824 *One* 7, e38115. <https://doi.org/10.1371/journal.pone.0038115>
- 825 Lovie, P., 1986. Identifying Outliers, in: Lovie, A.D. (Ed.), *New Developments in Statistics for Psychology*
826 *and the Social Sciences*. The British Psychological Society and Methuen, London, UK, pp. 44–69.
- 827 Mak, J.N., Wolpaw, J.R., 2009. Clinical Applications of Brain-Computer Interfaces: Current State and
828 Future Prospects. *Biomed. Eng. IEEE Rev.* 2, 187–199. <https://doi.org/10.1109/RBME.2009.2035356>
- 829 Mani, S., Pauly, J., Conolly, S., Meyer, C., Nishimura, D., 1997. Background suppression with multiple
830 inversion recovery nulling: Applications to projective angiography. *Magn. Reson. Med.* 37, 898–905.
831 <https://doi.org/10.1002/mrm.1910370615>
- 832 Mazziotta, J., Toga, A., Evans, A., Fox, P., Lancaster, J., Zilles, K., Woods, R., Paus, T., Simpson, G., Pike,
833 B., Holmes, C., Collins, L., Thompson, P., MacDonald, D., Iacoboni, M., Schormann, T., Amunts, K.,
834 Palomero-Gallagher, N., Geyer, S., Parsons, L., Narr, K., Kabani, N., Goualher, G. Le, Boomsma, D.,
835 Cannon, T., Kawashima, R., Mazoyer, B., 2001. A probabilistic atlas and reference system for the
836 human brain: International Consortium for Brain Mapping (ICBM). *Philos. Trans. R. Soc.*
837 *London. Series B Biol. Sci.* 356, 1293–1322. <https://doi.org/10.1098/rstb.2001.0915>
- 838 Mehler, D.M.A., Sokunbi, M.O., Habes, I., Barawi, K., Subramanian, L., Range, M., Evans, J., Hood, K.,
839 Lührs, M., Keedwell, P., Goebel, R., Linden, D.E.J., 2018. Targeting the affective brain—a randomized
840 controlled trial of real-time fMRI neurofeedback in patients with depression.
841 *Neuropsychopharmacology*. <https://doi.org/10.1038/s41386-018-0126-5>
- 842 Moray, N., 1959. Attention in dichotic listening: Affective cues and the influence of instructions. *Q. J. Exp.*
843 *Psychol.* 11, 56–60. <https://doi.org/10.1080/17470215908416289>
- 844 Mozzachiodi, R., Byrne, J.H., 2010. More than synaptic plasticity: role of nonsynaptic plasticity in learning
845 and memory. *Trends Neurosci.* 33, 17–26.
- 846 Mutsaerts, H.J.M.M., Steketee, R.M.E., Heijtel, D.F.R., Kuijter, J.P.A., van Osch, M.J.P., Majoie, C.B.L.M.,
847 Smits, M., Nederveen, A.J., 2014. Inter-Vendor Reproducibility of Pseudo-Continuous Arterial Spin
848 Labeling at 3 Tesla. *PLoS One* 9, e104108. <https://doi.org/10.1371/journal.pone.0104108>
- 849 Nichols, T., Holmes, A., 2003. Nonparametric Permutation Tests for Functional NeuroImaging, in: *Human*
850 *Brain Function: Second Edition*. pp. 887–910. <https://doi.org/10.1016/B978-012264841-0/50048-2>
- 851 Patriat, R., Molloy, E.K., Meier, T.B., Kirk, G.R., Nair, V.A., Meyerand, M.E., Prabhakaran, V., Birn, R.M.,
852 2013. The effect of resting condition on resting-state fMRI reliability and consistency: A comparison
853 between resting with eyes open, closed, and fixated. *NeuroImage* 78, 463–473.
854 <https://doi.org/10.1016/j.neuroImage.2013.04.013>
- 855 Roberts, L.E., Husain, F.T., Eggermont, J.J. 2013. Role of attention in the generation and modulation of
856 tinnitus. *Neurosci Biobehav Rev.* 37, 1754–73. <https://doi.org/10.1016/j.neubiorev.2013.07.007>
- 857 Saliba, J., Al-Reefi, M., Carriere, J.S., Verma, N., Provencal, C., Rappaport, J.M., 2016. Accuracy of
858 Mobile-Based Audiometry in the Evaluation of Hearing Loss in Quiet and Noisy Environments.
859 *Otolaryngol. Neck Surg.* 156, 706–711. <https://doi.org/10.1177/0194599816683663>
- 860 Scharnowski, F., Hutton, C., Josephs, O., Weiskopf, N., Rees, G., 2012. Improving Visual Perception
861 through Neurofeedback. *J. Neurosci.* 32, 17830–17841. <https://doi.org/10.1523/JNEUROSCI.6334-11.2012>
862

- 863 Schecklmann, M., Landgrebe, M., Poepl, T.B., Kreuzer, P., Männer, P., Marienhagen, J., Wack, D.S.,
 864 Kleinjung, T., Hajak, G., Langguth, B., 2013. Neural correlates of tinnitus duration and Distress: A
 865 positron emission tomography study. *Hum. Brain Mapp.* 34, 233–240.
- 866 Seydell-Greenwald, A., Leaver, A.M., Turesky, T.K., Morgan, S., Kim, H.J., Rauschecker, J.P., 2012.
 867 Functional MRI evidence for a role of ventral prefrontal cortex in tinnitus. *Adv. Neurosci. Tinnitus*
 868 1485, 22–39. <https://doi.org/http://dx.doi.org/10.1016/j.brainres.2012.08.052>
- 869 Sherwood, M.S., Kane, J.H., Weisend, M.P., Parker, J.G., 2016a. Enhanced control of dorsolateral prefrontal
 870 cortex neurophysiology with real-time functional magnetic resonance imaging (rt-fMRI) neurofeedback
 871 training and working memory practice. *NeuroImage* 124, 214–223.
 872 <https://doi.org/10.1016/j.neuroImage.2015.08.074>
- 873 Sherwood, M.S., Weisend, M.P., Kane, J.H., Parker, J.G., 2016b. Combining real-time fMRI neurofeedback
 874 training of the DLPFC with *n*-back practice results in neuroplastic effects confined to the neurofeedback
 875 target region. *Front. Behav. Neurosci.* 10(138), 1–9. <https://doi.org/10.3389/fnbeh.2016.00138>
- 876 Shinozaki, J., Harada, K., Nagahama, H., Sakurai, Y., Akatsuka, Y., Nagamine, T., Kochiyama, T., 2013. In
 877 the Range of 20 to 35ms, an Echo-time of 20ms is Preferred for 3-tesla Functional Magnetic Resonance
 878 Imaging. *Adv. Biomed. Eng.* 2, 47–54. <https://doi.org/10.14326/abe.2.47>
- 879 Silva, A.C., Kim, S.-G., 1999. Pseudo-continuous arterial spin labeling technique for measuring CBF
 880 dynamics with high temporal resolution. *Magn. Reson. Med.* 42, 425–429.
 881 [https://doi.org/10.1002/\(SICI\)1522-2594\(199909\)42:3<425::AID-MRM3>3.0.CO;2-S](https://doi.org/10.1002/(SICI)1522-2594(199909)42:3<425::AID-MRM3>3.0.CO;2-S)
- 882 Smith, S.M., 2002. Fast robust automated brain extraction. *Hum. Brain Mapp.* 17, 143–155.
 883 <https://doi.org/10.1002/hbm.10062>
- 884 Smith, S.M., Jenkinson, M., Woolrich, M.W., Beckmann, C.F., Behrens, T.E.J., Johansen-Berg, H.,
 885 Bannister, P.R., De Luca, M., Drobnjak, I., Flitney, D.E., Niazy, R.K., Saunders, J., Vickers, J., Zhang,
 886 Y., De Stefano, N., Brady, J.M., Matthews, P.M., 2004. Advances in functional and structural MR
 887 image analysis and implementation as FSL. *NeuroImage* 23, S208–S219.
 888 <https://doi.org/10.1016/j.neuroImage.2004.07.051>
- 889 Sorkin, R.D., 1999. Spreadsheet signal detection. *Behav. Res. Methods, Instruments, Comput.* 31, 46–54.
 890 <https://doi.org/10.3758/BF03207691>
- 891 Subramanian, L., Hindle, J. V, Johnston, S., Roberts, M. V, Husain, M., Goebel, R., Linden, D., 2011. Real-
 892 Time Functional Magnetic Resonance Imaging Neurofeedback for Treatment of Parkinson's Disease. *J.*
 893 *Neurosci.* 31, 16309–16317. <https://doi.org/10.1523/JNEUROSCI.3498-11.2011>
- 894 Sulzer, J., Haller, S., Scharnowski, F., Weiskopf, N., Birbaumer, N., Blefari, M.L., Bruehl, A.B., Cohen,
 895 L.G., DeCharms, R.C., Gassert, R., Goebel, R., Herwig, U., LaConte, S., Linden, D., Luft, A., Seifritz,
 896 E., Sitaram, R., 2013. Real-time fMRI neurofeedback: Progress and challenges. *NeuroImage* 76, 386–
 897 399. <https://doi.org/10.1016/j.neuroImage.2013.03.033>
- 898 Swets, J.A., Sewall, S.T., 1963. Invariance of signal detectability over stages of practice and levels of
 899 motivation. *J. Exp. Psychol.* 66, 120–126. <https://doi.org/10.1037/h0049098>
- 900 Thibault, R.T., MacPherson, A., Lifshitz, M., Roth, R.R., Raz, A., 2018. Neurofeedback with fMRI: A
 901 critical systematic review. *NeuroImage* 172, 786–807. <https://doi.org/10.1016/j.neuroimage.2017.12.071>
- 902 Thompson, G.P., Sladen, D.P., Borst, B.J.H., Still, O.L., 2015. Accuracy of a Tablet Audiometer for
 903 Measuring Behavioral Hearing Thresholds in a Clinical Population. *Otolaryngol. Neck Surg.* 153, 838–

842. <https://doi.org/10.1177/0194599815593737>
- 904
905 Vaughan, T.M., McFarland, D.J., Schalk, G., Sarnacki, W.A., Krusienski, D.J., Sellers, E.W., Wolpaw, J.R.,
906 2006. The wadsworth BCI research and development program: at home with BCI. *Neural Syst. Rehabil.*
907 *Eng. IEEE Trans.* 14, 229–233. <https://doi.org/10.1109/TNSRE.2006.875577>
- 908 Veit, R., Singh, V., Sitaram, R., Caria, A., Rauss, K., Birbaumer, N., 2012. Using real-time fMRI to learn
909 voluntary regulation of the anterior insula in the presence of threat-related stimuli. *Soc. Cogn. Affect.*
910 *Neurosci.* 7, 623–634. <https://doi.org/10.1093/scan/nsr061>
- 911 Wager, T.D., Lindquist, M.A., 2011. Essentials of Functional Magnetic Resonance Imaging, in: Decety, J.,
912 Cacioppo, J.T. (Eds.), *The Oxford Handbook of Social Neuroscience*. Oxford University Press, pp. 69–
913 96.
- 914 Wang, H., Tian, J., Yin, D., Jiang, S., Yang, W., Han, D., Yao, S., Shao, M., 2001. Regional glucose
915 metabolic increases in left auditory cortex in tinnitus patients: a preliminary study with positron
916 emission tomography. *Chin. Med. J. (Engl.)* 114, 848–851.
- 917 Weiskopf, N., Sitaram, R., Josephs, O., Veit, R., Scharnowski, F., Goebel, R., Birbaumer, N., Deichmann,
918 R., Mathiak, K., 2007. Real-time functional magnetic resonance imaging: methods and applications.
919 *Proc. Int. Sch. Magn. Reson. Brain Funct. Proc. Int. Sch. Magn. Reson. Brain Funct.* 25, 989–1003.
920 <https://doi.org/10.1016/j.mri.2007.02.007>
- 921 Winkler, A.M., Ridgway, G.R., Webster, M.A., Smith, S.M., Nichols, T.E., 2014. *NeuroImage* 92, 381–397.
922 <https://doi.org/10.1016/J.NEUROIMAGE.2014.01.060>
- 923 Woolrich, M.W., Jbabdi, S., Patenaude, B., Chappell, M., Makni, S., Behrens, T., Beckmann, C., Jenkinson,
924 M., Smith, S.M., 2009. Bayesian analysis of neuroImaging data in FSL. *NeuroImage* 45, S173–S186.
925 <https://doi.org/10.1016/j.neuroImage.2008.10.055>
- 926 Xu, G., Rowley, H.A., Wu, G., Alsop, D.C., Shankaranarayanan, A., Dowling, M., Christian, B.T., Oakes,
927 T.R., Johnson, S.C., 2010. Reliability and Precision of Pseudo-Continuous Arterial Spin Labeling
928 Perfusion MRI on 3.0 T and Comparison with ¹⁵O-Water PET in Elderly Subjects At Risk for
929 Alzheimer’s Disease. *NMR Biomed.* 23, 286–293. <https://doi.org/10.1002/nbm.1462>
- 930 Ye, F.Q., Frank, J.A., Weinberger, D.R., McLaughlin, A.C., 2000. Noise reduction in 3D perfusion imaging
931 by attenuating the static signal in arterial spin tagging (ASSIST). *Magn. Reson. Med.* 44, 92–100.
932 [https://doi.org/10.1002/1522-2594\(200007\)44:1<92::AID-MRM14>3.0.CO;2-M](https://doi.org/10.1002/1522-2594(200007)44:1<92::AID-MRM14>3.0.CO;2-M)
- 933 Yoo, S.-S., O’Leary, H.M., Fairney, T., Chen, N.-K., Panych, L.P., Park, H., Jolesz, F.A., 2006. Increasing
934 cortical activity in auditory areas through neurofeedback functional magnetic resonance imaging.
935 *Neuroreport* 17, 1273–1278.
- 936 Young, K.D., Zotev, V., Phillips, R., Misaki, M., Yuan, H., Drevets, W.C., Bodurka, J., 2014. Real-Time
937 fMRI Neurofeedback Training of Amygdala Activity in Patients with Major Depressive Disorder. *PLoS*
938 *One* 9, e88785.
- 939 Yuan, H., Young, K.D., Phillips, R., Zotev, V., Misaki, M., Bodurka, J., 2014. Resting-State Functional
940 Connectivity Modulation and Sustained Changes After Real-Time Functional Magnetic Resonance
941 Imaging Neurofeedback Training in Depression. *Brain Connect.* 4, 690–701.
942 <https://doi.org/10.1089/brain.2014.0262>
- 943 Zhang, G., Yao, L., Zhang, H., Long, Z., Zhao, X., 2013. Improved Working Memory Performance through
944 Self-Regulation of Dorsal Lateral Prefrontal Cortex Activation Using Real-Time fMRI. *PLoS One* 8,

945 e73735. <https://doi.org/10.1371/journal.pone.0073735>

946 Zhang, S., Yoshida, W., Mano, H., Yanagisawa, T., Shibata, K., Kawato, M., Seymour, B., 2018.
947 Endogenous controllability of closed-loop brain-machine interfaces for pain. bioRxiv.

948

ACCEPTED MANUSCRIPT